Swiss J Geosci (2011) 104:31–54
DOI 10.1007/s00015-010-0050-0

Late Alpine brittle faulting in the Rotondo granite (Switzerland): deformation mechanisms and fault evolution

Volker Lützenkirchen · Simon Loew

Received: 13 November 2009 / Accepted: 15 November 2010 / Published online: 27 January 2011

Abstract The unlined Bedretto tunnel in the Central Swiss Alps has been used to investigate in detail the fault architecture and late Alpine brittle faulting processes in the Rotondo granite on macroscopic and microscopic scales. Brittle faults in the late Variscan Rotondo granite preferentially are situated within the extent of preexisting ductile shear zones. Only in relatively few cases the damage zone extends into or develops in the previously undeformed granite. Slickensides suggest a predominant (dextral) strike-slip movement along these steeply dipping and NE–SW-striking faults. Microstructures of these fault rocks illustrate a multi-stage retrograde deformation history from ductile to brittle conditions up to the cessation of fault activity. In addition these fabrics allow identifying cataclastic flow, fluid-assisted brecciation and chemical corrosive wear as important deformation mechanisms during this retrogressive deformation path. Based on the analysis of zeolite microfabrics (laumontite and stilbite; hydrated Ca–Al- and Na–Ca–Al–silicate, respectively) in fault breccias, cataclasites and open fractures we conclude, that the main phase of active brittle faulting started below 280°C and ceased ca. 14 Ma ago at temperatures slightly above 200°C. This corresponds to a depth of approx. 7 km.

Editorial handling: A. G. Milnes.

V. Lützenkirchen (✉)
Matousek, Baumann & Niggli AG, Mäderstrasse 8,
5400 Baden, Switzerland
e-mail: luetzenk@gmx.net

S. Loew
Swiss Federal Institute of Technology (ETH Zurich),
Sonneggstrasse 5, 8092 Zurich, Switzerland

Keywords Fault · Gotthard massif · Rotondo · Granite · Zeolite · *P–T*-evolution

1 Introduction

Faults and heavily fractured rocks are a main cause for geological hazards in hard rock tunnel construction. Such hazards are related to high groundwater inflows, structurally controlled instabilities and squeezing ground leading to slow excavation advance rates and high costs (Jamier 1975; Maréchal 1998; Buergi et al. 1999; Heer and Jakob 1999; Loew et al. 2007; Loew et al. 2010). In crystalline rocks brittle faults, damage zones and single joints act as preferential water conducting structures (Brace 1980; Barton et al. 1995; Evans et al. 1997; Caine and Forster 1999) which also have a significant impact on groundwater management, geothermal energy and the performance of deep nuclear waste repositories (e.g. Krasny and Sharp 2007). Predicting the mechanical and hydraulic behaviour of fault rocks at project relevant scales is substantially improved, when the internal architecture, mineralogy and formation history of fault rocks is understood. This is why a combined analysis of fault rock genesis and hydraulic properties has been carried out in an unlined tunnel of the Gotthard massif in the Central Alps (Lützenkirchen 2002).

The central Swiss Alps consist of three uplifted crystalline bodies of the European continental crust: the so-called external crystalline "massifs" of Aar, Tavetsch and Gotthard (Fig. 1). In these massifs several investigations on ductile shear zones and brittle fault zones have recently been carried out. Laws et al. (2003), Wyder and Mullis (1998), and Zangerl et al. (2006) analysed the geometric, structural and geomechanical properties of ductile shear zones and brittle faults in the central Aar, Tavetsch and

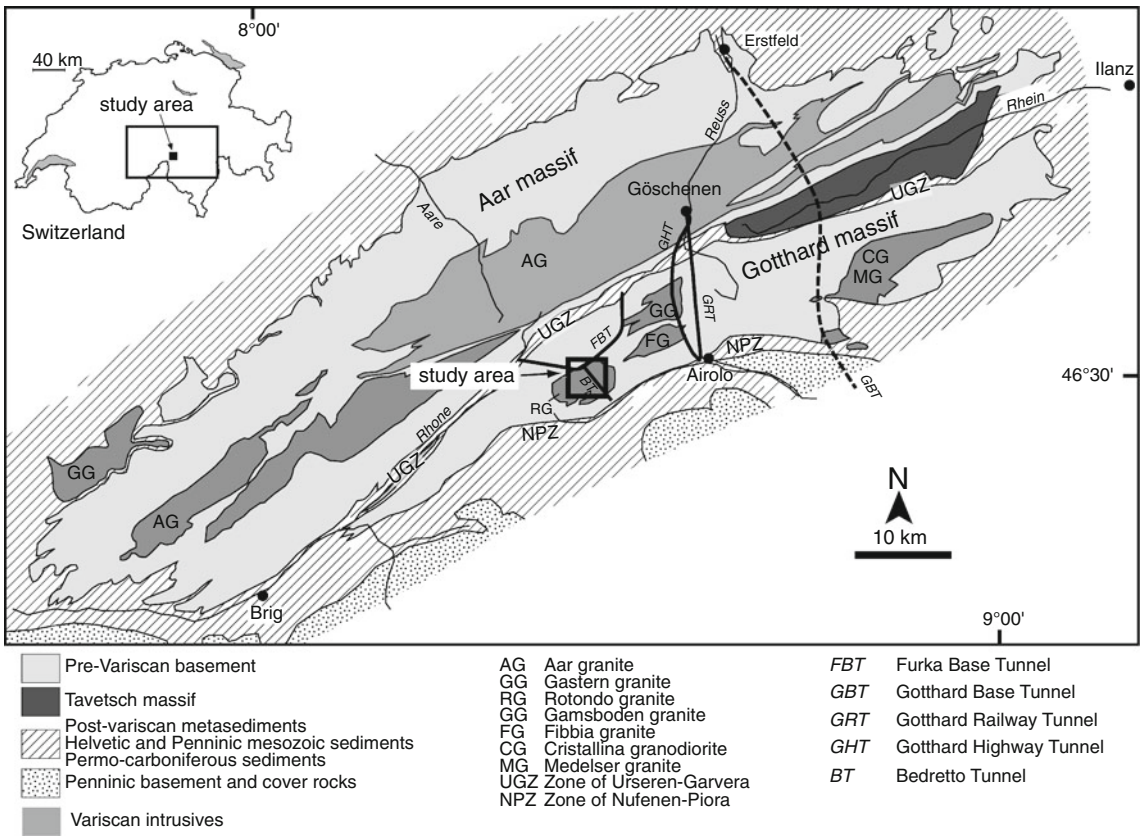

Fig. 1 Geographical and geological overview of the Gotthard and Aar massif after Zangerl et al. (2006), showing the location of the study area, the Furka base tunnel und other tunnels mentioned in the text

Gotthard massif, respectively. The hydrogeologic properties of fault zones were investigated by Frei and Loew (2001) in the southern Aar massif and by Lützenkirchen (2002) in the central and eastern Gotthard massif, the latter work representing the basis for this paper.

In a few cases fault rocks in the Gotthard and Aar massifs have been dated. Kralik et al. (1992) analysed fault gouge and mylonite material from the Grimsel Underground Research Laboratory in the Aar-massif using Rb-Sb, K-Ar and ^{3}H isotope techniques. Fault activity occurred at >25 Ma (>400°C), 20–18 Ma (350–300°C), 10 Ma (190°C) and 6 Ma (170–120°C). Jäckli (1951, 1957) observed fault scarps running parallel to the northern slopes of the upper Vorderrhein valley (southern Aar massif) that locally offset late glacial moraines, suggesting neotectonic or gravitational slope movements in the last 12 ka. Other authors reported complementary observations on similar fault systems in the area, such as (Eckardt 1957; Steck 1968; Eckardt et al. 1983; Fischer 1990; Frei and Loew 2001; Laws 2001; Lützenkirchen 2002; Persaud and Pfiffner 2004).

The formation of fault rock is the result of the interaction of brittle mechanical deformation processes and syn-kinematic mineral reactions (e.g. Passchier and Trouw 2005), both depending on *P–T*-conditions, stress and strain rate, availability and chemical composition of fluids, permeability, mineralogy and mechanical properties of the host rock (Chester et al. 1993; Sibson 2000). These conditions may considerably vary spatially as well as temporarily, typically resulting in a complex and ambiguous record of deformation history. In contrast to deformation in prograde metamorphic conditions, the determination of retrograde deformation processes and conditions is largely hampered by the inertia of mineral reactions under low temperatures and by the mechanical disintegration of older, pre-existing minerals and structures.

However, under favourable conditions with regard to mineral assemblages, local deformation history and available outcrops of fault rocks, the complex deformation history of faults and according *P–T*-conditions can be determined based on mineralogical and microstructural observations. Such favourable conditions are present in the Variscan Rotondo granite of the Gotthard massif, especially in an unlined access drift of the Furka base tunnel, providing spectacular insights into late Alpine stages of brittle faulting. In this paper, we characterise in detail different types of faults and fault rocks of the Rotondo granite from the field scale (m-100 m) to the micro-scale

(mm-cm). The link between the structural development of these faults and regional tectonic history is assessed through detailed mineralogical and microstructural observations that give insight into brittle deformation processes and the corresponding *P–T*-conditions. The hydraulic properties of these faults are discussed in Lützenkirchen (2002) and a subsequent paper.

2 Geological setting

The crystalline basement rocks of Aar, Gotthard and Tavetsch massifs (Fig. 1) were traditionally considered to represent largely immobile basement blocks of the European continental crust, only weakly affected by Alpine nappe tectonics. As first suggested by Milnes (1974) the Gotthard and Tavetsch massifs today are considered Subpenninic nappes (Schmid et al. 2004) or Helvetic (Pfiffner 2009), representing basement units of the Helvetic nappes. For simplicity we will keep the term "massif", although these units are strongly deformed and thrust in northward direction.

The Gotthard massif extends about 80 km in WSW–ESE direction and about 10 km in N–S direction (Fig. 1). The northern boundary of the Gotthard massif is defined by the autochthonous sediment cover of the Urseren-Gavera-Zone (Wyss 1985). The Penninic gneisses south of the Gotthard massif are separated from the Gotthard massif by Mesozoic rocks of the narrow E-W-striking Nufenen-Piora-Scopi zone (Liszkay 1965; Leu 1985; Klaper and Bucher-Nurminen 1987; Kamber 1993).

The investigation area is located at the upper end of the SW–NE trending Geren valley 10 km west of the Gotthard pass (Figs. 1, 2). The surface of this high alpine region is characterised by a steep morphology and a largely absent vegetation cover. The Pizzo Rotondo (3,192 m a.s.l) represents the highest, partially glaciated peak in the region.

In the late 1970s, the 14.9 km long Furka railway base tunnel was built connecting the Urseren valley (canton of Uri, Fig. 1) in the east with the upper Rhone valley in the west (Obergoms, canton of Valais). The Bedretto tunnel was built as an auxiliary access drift (Figs. 2, 3), being abandoned after completion of the Furka base tunnel. The portal of the 5.2 km long Bedretto tunnel is located close to the village of Ronco in the Ticino valley south-west of the Piz Rotondo. This tunnel of approximately 3 m diameter is still accessible between the window in the Furka tunnel (Tkm 5218: Tkm refers to tunnel chainage) and tunnel station Tkm 3775, where the tunnel completely collapsed within a fault zone. In this accessible part of the tunnel the overburden ranges between 1,000 and 1,300 m.

The tunnel walls are predominantly unlined; weak (fault-) zones are only partially supported by steel arches and timber works. Very few supported tunnel sections have also been covered by shotcrete. Therefore, the Bedretto tunnel offers a great opportunity to study the structural geology, hydrogeology and rock mechanical behaviour of faults.

The faults zones and fault rocks discussed in this paper are situated within the extent of the dome-shaped, late Variscan Rotondo granite surrounding the Pizzo Rotondo (Fig. 2). This granite has an 8 km long tail of a few hundred meters width east of the Pizzo Rotondo reaching as far as the Gotthard pass (Hafner et al. 1975).

The Rotondo granite intruded the Paleozoic polymetamorphic crystalline basement rocks of the Gotthard massif at 294.3 ± 1.1 Ma (Sergeev and Steiger 1995) in a late phase of the Variscan orogeny and underwent amphibolite

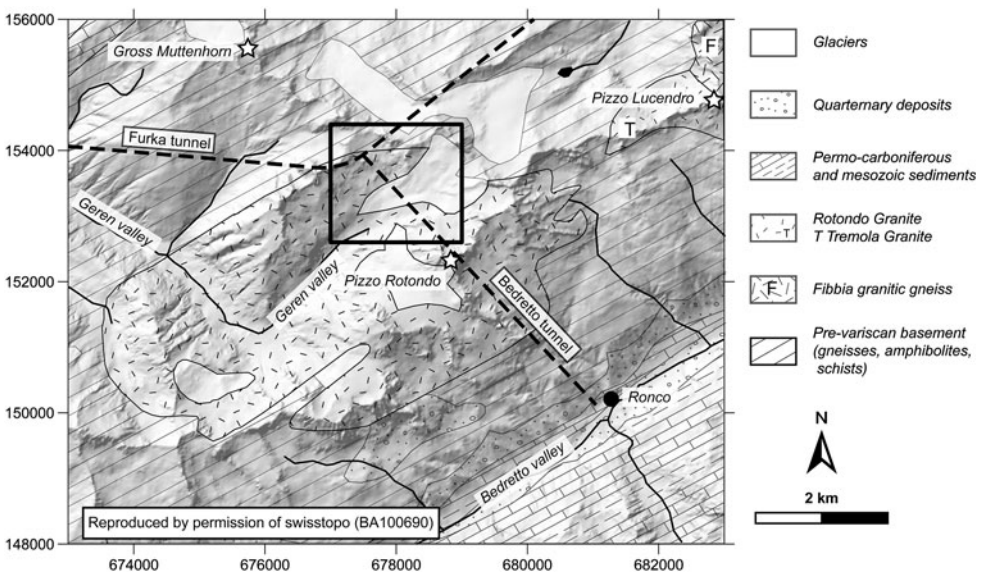

Fig. 2 Geological sketch of the region of the Bedretto tunnel. See text for explanations. The *box* in the centre indicates the position of the detailed map shown in Fig. 3

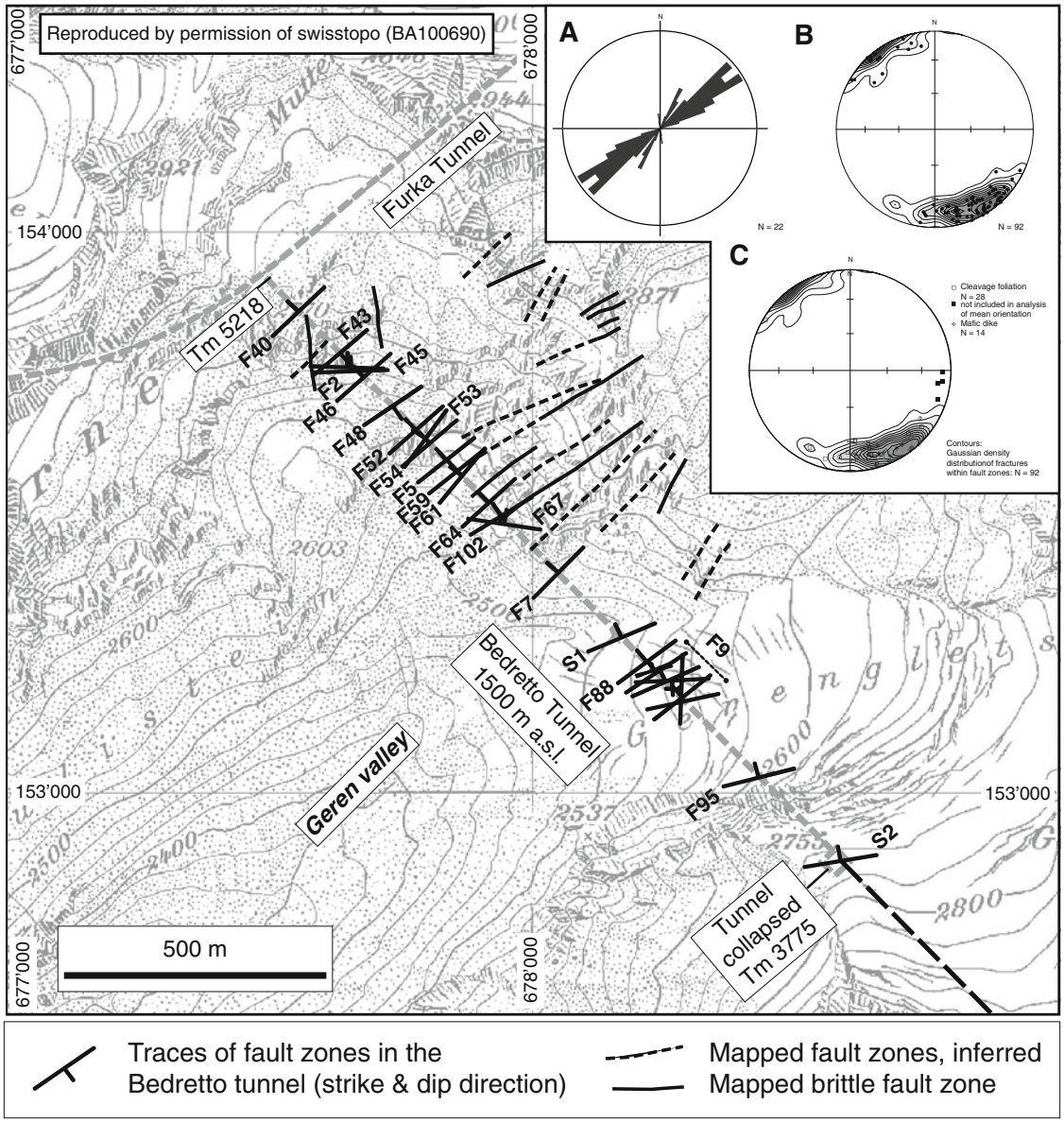

Fig. 3 Faults mapped at the surface above the Bedretto tunnel and orientations of selected faults (*Fxx*) in the Bedretto tunnel more than 1,000 m underneath. *Short lines* crossing the Bedretto tunnel indicate traces of faults in the tunnel as recorded by Schneider (1985). **a** Rose diagram of faults mapped at the surface, mean strike: 50°, **b** Schmidt's net (*lower hemisphere*) of fault orientation in the tunnel between Tm 3,500 and 5,218 (Rotondo granite). Mean weighted (see Priest 1993 for procedure) orientation: 326/85 (azimuth of dip direction/dip angle), according mean strike: 56°. **c** Orientation of lamprophyre dikes (335/77) and shear zones/cleavage (349/74), same tunnel section, data by Schneider (1979)

facies overprint during the Variscan metamorphism (Nunes and Steiger 1974; Oberhänsli et al. 1988). Mafic and granitic dikes are ubiquitous in the Gotthard massif (Oberhaensli 1985); most of the dikes encountered in the Bedretto tunnel are lamprophyres. In comparison to older Variscan intrusions within the Gotthard massif like the nearby Gamsboden and Fibbia granitic gneiss (300–298 Ma, Schaltegger and Corfu 1992) the Rotondo granite was less affected by Variscan compressional deformation (Mercolli et al. 1994), resulting in a generally weakly developed Variscan foliation composed of preferred mineral orientations and flattening of quartz grains. Guerrot and Steiger (1991) thus postulate a Variscan deformation phase between the intrusion of the older Gamsboden and Fibbia granitic gneisses and the intrusion of the Rotondo granite.

During the Tertiary Alpine compression the Mesozoic sedimentary cover of the Gotthard massif (the Helvetic and Ultrahelvetic nappes) was for the most part detached [according to Schmid et al. (1996) in the upper Eocene Cavistrau phase at ca. 38 Ma] leaving behind the

metasedimentary zones of Nufenen-Piora-Scopi at the southern margin of the Gotthard massif, and the zone of Urseren-Garvera at its northern one. Later (during the lower Oligocene Calanda phase) maximum *P–T*-conditions of Alpine greenschist facies metamorphism (Frey et al. 1980; Frey and Mählmann 1999) were attained. The Rotondo granite is located south of the microcline/sanidine-isograde (Bernotat and Bambauer 1980) and north of the staurolith-isograde (Niggli 1970). Bernotat and Bambauer (1980) estimated peak temperatures slightly above 450°C. The corresponding Alpine cleavage developed preferentially in narrow SW–NE trending ductile shear zones within the massif and at the massif's margins including the post-Variscan sediments (Arnold 1970). In the lower Miocene the Gotthard massif [according to Schmid et al. (1996) at ~20 Ma] and later the southern Aar massif [according to Wyder and Mullis (1998) between ca. 17–13 Ma] were backfolded, rotating the main tectonic boundaries, foliation and shear zones, respectively, into a subvertical orientation.

As a result, the main structural elements in the Rotondo area as well as in the western and central Gotthard massif are striking SW–NE, almost paralleling the massif's northern and southern margins. The steeply dipping foliation forms a fan along a NW–SE profile (Zangerl et al. 2006). The Bedretto tunnel is situated close to the culmination; here the cleavage dips about vertically.

3 Fault zones and deformation mechanisms

3.1 Classification of fault rock

The nomenclature of fault rocks has been a matter of debate since the 1960s [see historical overwiew and discussion in Snoke et al. (1998); see also new approach in Woodcock and Mort (2008)]. The main controversy is whether to apply genetic terms in the description of fault rock e.g. in the field, though the deformation mechanisms being responsible for the observed fabric may be not known or incorrectly inferred. As recommended by Snoke et al. (1998), we apply the classification of Scholz (1990), representing a modified textural—thus descriptive—classification based on Sibson (1977). Fault rocks are distinguished by their fabric (random fabric/foliated) and by their cohesion (incohesive/cohesive).

Since by far most of the fabrics observed in fault rock of the Rotondo granite show no or hardly any foliation, the description of the fault rock classification applied in this paper can be restrained primarily to fault rock showing random fabric: Incohesive fault rock with >30% visible fragments of rock mass is called fault breccia, whereas incohesive fault rock containing <30% rock fragments is named fault gouge. Fine grained fault rock showing a foliation have been observed (Chester et al. 1985), representing a foliated gouge (<30% rock fragments). Cohesive fault rock is subdivided into pseudotachylyte (glass-devitrified glass; not found in our study), crush breccia (fragments >0.5 cm), fine crush breccia (0.1 < fragments < 0.5 cm), crush microbreccia (fragments <0.1 cm) and the cataclasite series. Cataclasites are further subdivided into protocataclasite, cataclasite and ultracataclasite.

3.2 Structural elements of fault zones

According to Caine et al. (1996) fault zones can be characterised by a fault core, a damage zone and the protolith. Most of the displacement within a fault zone is accommodated in the fault core, thus being intensely fractured, brecciated, and geochemically altered. In most cases the fault core comprises a clay-rich gouge zone. The adjacent damage zone represents a network of subsidiary fractures, veins and small faults. The protolith or country rock is characterised by hardly any evidence of brittle deformation except for joints.

3.3 Deformation mechanisms

Deformation mechanisms depend on physical conditions, strain rate, mineralogy and mechanical properties of the rock. In quartzo-feldspathic rocks at temperatures >300–350°C (Sibson 1977) strain is for the most part accommodated by crystal plasticity, including processes like pressure solution, intracrystalline deformation, dynamic recrystallisation, grain boundary sliding and twinning (Passchier and Trouw 2005). Resulting fabrics are typically foliations made up by mica showing a preferred orientation, or a separation into recrystallised bands and ribbons of quartz and feldspar, elongated blasts or grains.

The presence of fractures on both the grain scale (microscopic) as well as on the macro-scale (>cm) indicates brittle deformation (cataclasis) at lower temperatures and/or high strain rates. On the macro-scale, processes such as the nucleation and propagation of fractures are characteristic. On the microscale, brittle deformation processes basically are microcracking and frictional sliding, including subcritical microcrack propagation (Blenkinsop 2000). Resulting structures include microcracks (mainly intragranular or transgranular), and microfaults containing grain fragments and deformation bands. Microstructures characterised by ±continuously distributed fractures and displacements of fragments are called cataclastic flow, occurring at higher confining pressures. The resulting microfabrics largely depend on the degree of mechanical comminution and the mineralogical composition of the host rock. The resulting fabrics may show crushed angular

rock or mineral fragments as well as fine grained, most intensely comminuted gouge material, which may represent a matrix for rock fragments. Foliation due to the parallel alignment of mica (Chester et al. 1985; Kanaori et al. 1991) may be developed in gouge material, or may be lacking and no orientation-preferred fabric can be observed. Chemical alteration is usually involved in brittle deformation. It may enhance sub-critical microcrack growth along cleavage microcracks in feldspars (Blenkinsop and Sibson 1992).

Syn-deformational recrystallisation and pressure solution may also occur to a minor extent in (semi-) brittle fault rock (Snoke et al. 1998). Crystalline rocks exhibiting brittle deformation features usually have been uplifted from depths where conditions typical for ductile deformation processes prevailed (>10–15 km, >250–350°C, Sibson 1977). Provided ongoing deformation along during uplifting, ductile and brittle features may occur within the same fault as a result of brittle deformation overprinting pre-existing ductile shear zones. Besides this succession of processes, ductile and brittle structures may also be generated simultaneously under certain conditions: a polymineralic rock may exhibit fractured grains in a ductily deformed matrix as a result of different rheological behaviour of minerals, e.g. quartz and feldspars (Tullis and Yund 1987; Gapais 1989; Stünitz and Fitz Gerald 1993).

4 Ductile shear zones and brittle faults in the Rotondo granite

4.1 Mineralogy and foliation

The Rotondo granite is a homogenous, massive light grey granite containing few blocks of xenolithic gneisses of less than a few meter extent. The subvertical, NE–SW striking foliation is only weakly developed, particularly in the southern part of the intrusion body (Labhart 2005) shown in Fig. 2. It is still a matter of debate whether this penetrative foliation (composed of preferred mineral orientations and quartz grain flattening) has to be considered late-Variscan or Alpine, see, for instance, Guerrot and Steiger (1991), Labhart (2005); see also the comments of Marquer (1990) for the Fibbia granite gneiss east of the Rotondo area and the comments of Arnold (1970) on penetrative Variscan foliation and Alpine cleavage in shear zones in the eastern Gotthard massif. We tend to attribute the weakly developed penetrative foliation to the late Variscan deformation, whereas Alpine cleavage preferentially developed in discrete shear zones. Within the area of investigation the penetrative foliation as well as the Alpine shear zones strike about massif-parallel in WSW–ENE direction (see Fig. 3).

The major mineral components of the Rotondo granite are plagioclase, alkali-feldspar, quartz, white mica and biotite (Fig. 4), representing a typical granoblastic granitic mineral assemblage (Hafner 1958). Plagioclase (albite) is very abundant, showing typical twins on the albite law and an anorthite-content of <15%. The perthitic alkali feldspars show exsolutions of low-albite and cross hatched twinning of microclines. Orthoclase as predominating alkali feldspar is less abundant, sometimes forming large blasts and occasionally showing twins on the Karlsbad law. According to Labhart (1977) the biotite content is relatively low (3–5%). Epidote/clinozoisite, chlorite, zircone, titanite, and carbonate are present as accessory minerals. Amongst opaque ore minerals pyrite is most abundant.

4.2 Ductile shear zones

Ductile shear zones in tunnel outcrops show darker colours compared to the host rock due to a higher content of biotite and/or reduced grain sizes. The orientation of these shear zones as shown in Fig. 3c has not

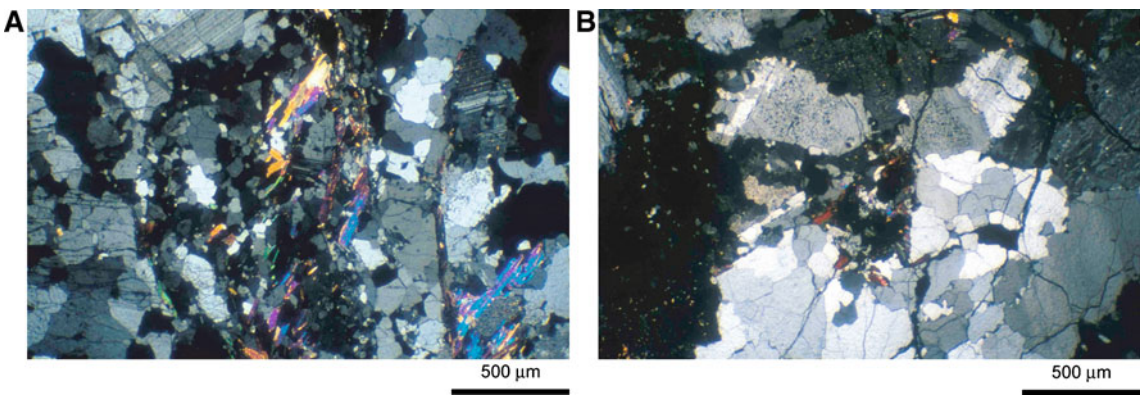

Fig. 4 Rotondo granite adjacent to faults, slightly foliated and showing microcracks. **a** Sample S2-1, **b** F2-B. *Crossed nicols*

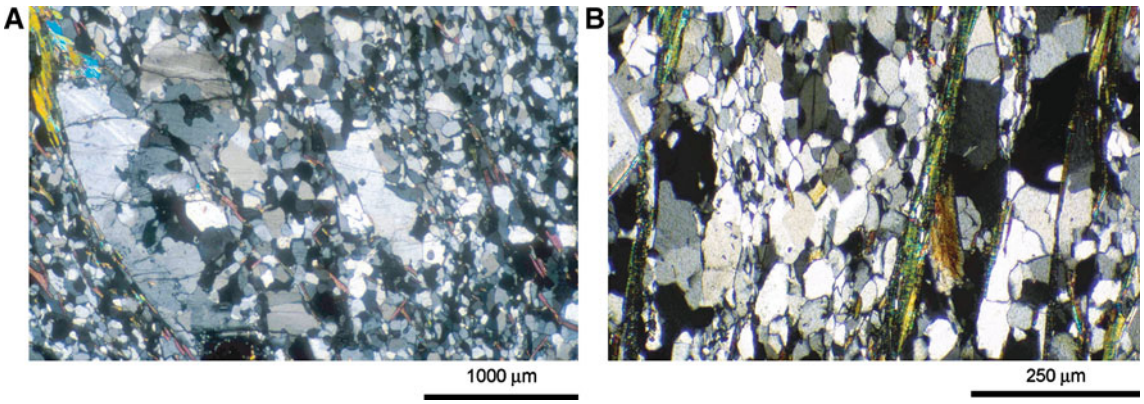

Fig. 5 Foliated Rotondo granite sampled from a ductile shear zone. **a** F40 A, **b** F102-6. *Crossed nicols*

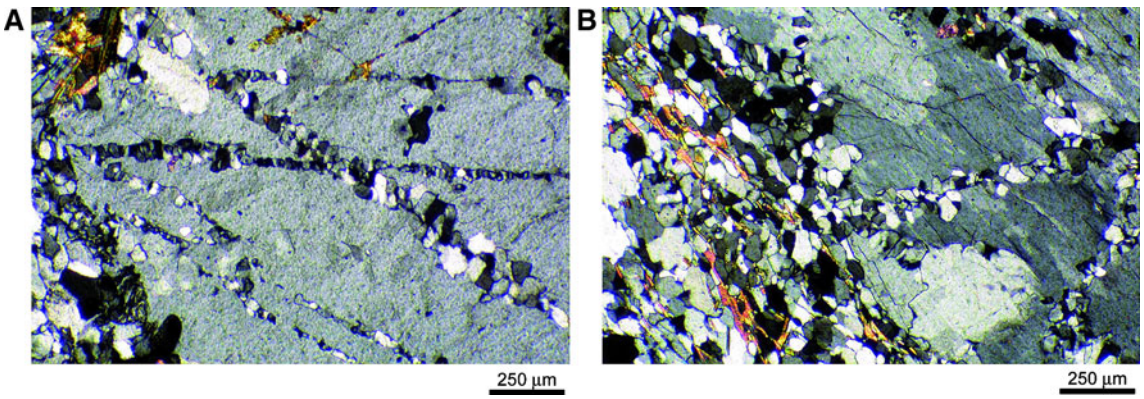

Fig. 6 Quartz-recrystallisates in feldspars. **a**, **b** F40-3. *Crossed nicols*

been measured systematically, but they are parallel to the main foliation and strike WSW–ENE. The transition from non- or weakly foliated host rock to shear zones is always gradual.

In comparison to the granite protolith, shear zones show a higher content of quartz and albite, relics of alkali feldspar along with mica and biotite. Chlorite and other accessory minerals may also be present in higher contents. Ductile shear zones are described in detail by Zangerl et al. 2006, and Marquer (1990); they show typically recrystallized domains of fine grained feldspar and quartz, and quartz-ribbons paralleling the foliation, which is made up primarily of mica and green to brown biotite (Fig. 5b). Few relictic domains of granitic fabric or feldspar blasts are present (Fig. 5a).

Thin bands of recrystallized quartz occasionally have been observed in large blasts of alkali feldspars (Fig. 6). These bands tend to form subparallel sets and occasionally constitute conjugate patterns. They are interpreted as brittle fractures in feldspars healed with quartz.

4.3 Brittle faults and fault zones

4.3.1 Fault orientation and spacing

Faults may occur on different scales: the faults that have been mapped in the Bedretto tunnel and at the surface have a total width including damage zones ranging from of several tens of centimetres to several meters. In the Bedretto tunnel the thickness of the fault core rarely exceeds a few decimetres. Fault zones are defined here as a tabular region containing many parallel or anastomosing faults.

Faults have also been mapped at ground surface between 2,500 and 2,900 m a.s.l., NE of the accessible part of the Bedretto tunnel (Fig. 3). In mountainous terrain composed of massive crystalline rock such steeply dipping faults and fault zones are often exposed as linear morphological depressions or scarps, because the cataclastic deformation of the host rock leads to the formation of weak fault rocks being prone to weathering and erosion. The opposite case that indurated and welded fault rock may appear as erosion-resistant ridges has

not been observed within the region (Lützenkirchen 2002; Zangerl et al. 2006). Some fault scarps could be identified at the ridge NE of this tunnel section, which exhibit few outcrops of fault rock. However, debris often covers outcrops of fault zones, so that despite ubiquitous fault scarps in the Rotondo-area actual outcrops of fault rocks at the surface are rare. Moreover, ductile shear zones may cause similar scarps (Laws 2001). The resulting map of Fig. 3 shows traces of fault zones showing at least one outcrop containing fault rock, and inferred faults and fault zones mapped by means of typical fault scarps suggesting the presence of a fault. In the same figure a rose diagrams of these mapped faults and a Schmidt's net showing the fracture orientation of fault zones measured in the Bedretto tunnel (data based on Schneider 1985). The mean strike of faults mapped at the surface is 50° (Fig. 3a), the weighted mean orientation (the tunnel represents the scanline, Priest 1993) of faults cropping out in the tunnel underneath is 326/85 (Fig. 3b, equal area Gaussian contour plot), the according mean strike is 56°. The mean orientation of the 15 mafic dikes in the Bedretto tunnel is 335/77 (Fig. 3c, data based on Schneider 1985). The cleavage, mainly measured within shear zones, shows a mean orientation of 349/74 (Fig. 3c, data based on Schneider 1985).

Maps of fault zones in the area of the Gotthard pass (about 10 km east of the Bedretto tunnel), provided by Lützenkirchen (2002) and Zangerl et al. (2006), show predominant SW–NE to WSW–ENE striking fault orientations, their mean orientation being consistent with the orientation of fault zones in the Rotondo granite at the surface above and in the Bedretto tunnel. In contrast to the Gotthard pass and east of it (Lützenkirchen 2002), no clear conjugate set of faults can be observed in the Rotondo granite. Very few faults and brittle fractures have orientations clearly deviating from the mean orientation (Fig. 3).

The Bedretto tunnel represents an excellent scanline for the determination of spacing of mapped faults in the Rotondo granite. Brittle structures indicated as "brittle shear fractures" and "faults" in Schneider (1985) were used to calculate the normal set spacing according to Priest (1993). For the entire Bedretto tunnel, the mean spacing of such faults amounts to 31.8 m (frequency $\approx$ 0.03), with the northern part of the Rotondo granite being clearly more intensely faulted: The normal set spacing is 15.0 m between tunnel meters 3,750 and 5,218 and 84.5 m in the southern section between 1,138 and 3,750 m.

Most slickenside striations on polished shear planes have low plunge angles of $\leq$30° (=8%, Fig. 7a). A unique determination of shear sense was not possible mainly because in homogeneous granite clear macroscopic offset markers are missing. Observations in the area of the Gotthard pass (Zangerl et al. 2006) show a predominant right-lateral shear sense for NE–SW to ENE–WSW-trending faults.

4.3.2 Fault architecture

Within the accessible section of the Bedretto tunnel, 79 faults and fault zones have been mapped by Schneider (1985). About 15 of them have been chosen for detailed analysis of the fault architecture, mineralogy und fault rock microstructures. The fault F64 is shown in a photograph in Fig. 8 as example. Detailed sketches auf fault outcrops are shown in Figs. 9, 10, 11, 12.

Several types of fault zones can be distinguished:

1. Faults within ductile shear zones
   A. Faults completely situated within a ductile shear zone always showing a central fault core and at least a narrow damage zone. Only in few cases

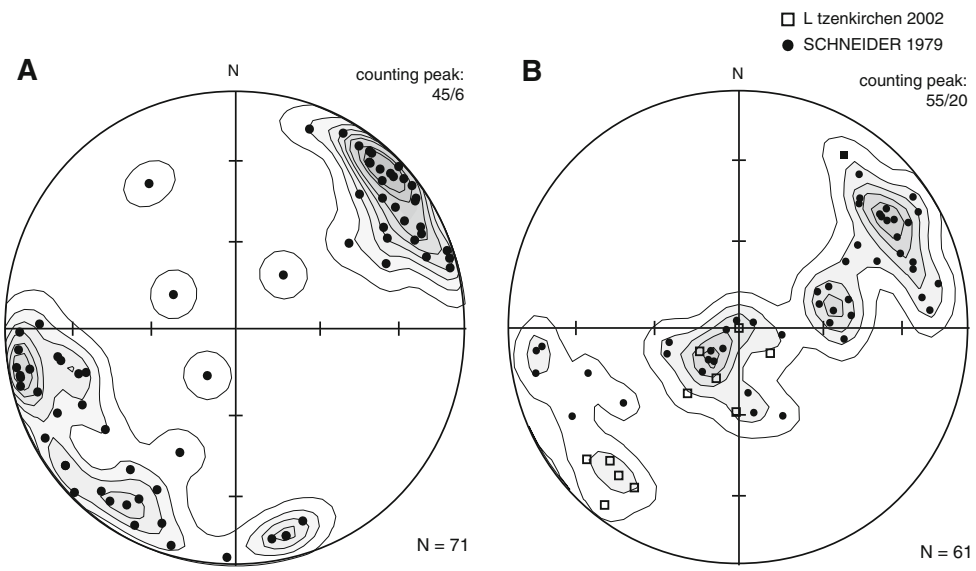

Fig. 7 **a** Schmidt's net (*lower hemisphere*) of slickenside striations in the Bedretto tunnel, **b** slickenside striations in the Gotthard highway tunnel 10 km east of the Bedretto tunnel [measured by Schneider (1979) and own measurements]

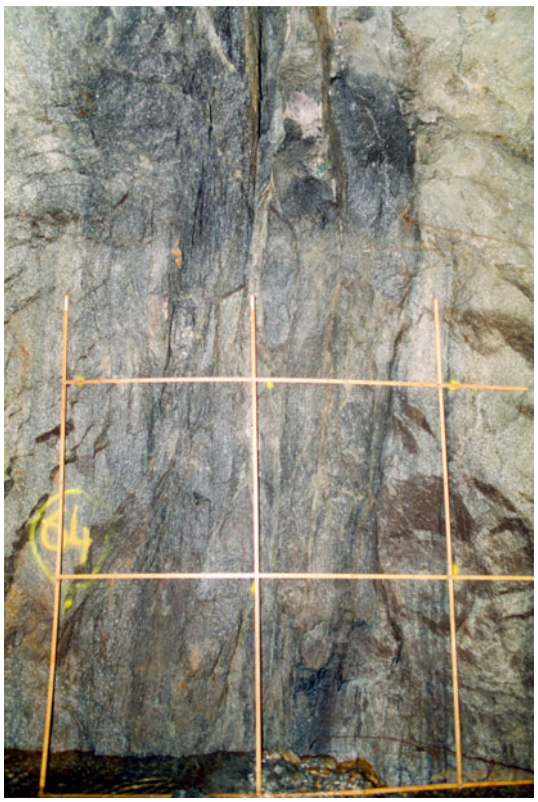

Fig. 8 Photograph of fault F64 at Tm 4,670, including a 1 m-grid scale

their damage zones considerably exceed the thickness of the central ductile shear zone. Within the fault core fault breccia and fault gouges of up to 10 cm (maximum 30 cm) thickness is present; in the intensely fractured damage zone cataclasites predominate. About 68% of the analysed fault zones belong to this type. Two examples are shown in Fig. 9 (refer to Fig. 3 for location).

B. Faults showing well developed damage zones larger than the ductile shear zone containing the fault core (8% of all analysed fault zones). These damage zones are characterised by few persistent and in many cases planar fractures, which are connected to a network of subsidiary and occasionally curved splay fractures. Thin bands of fine grained light grey or white fault breccia and fault gouges of a few centimeters width are ubiquitous. Cataclasites adjacent to persistent fractures are in most cases dissected by microfractures. The total width of the damage zones of such fault zones is mostly in the order of a few meters, in one exceptional case it is more than 50 m wide (example fault zone F9, Fig. 10).

2. Faults outside ductile shear zones

A. Fault (fracture zone) developed in essentially undeformed granite lacking a clearly developed

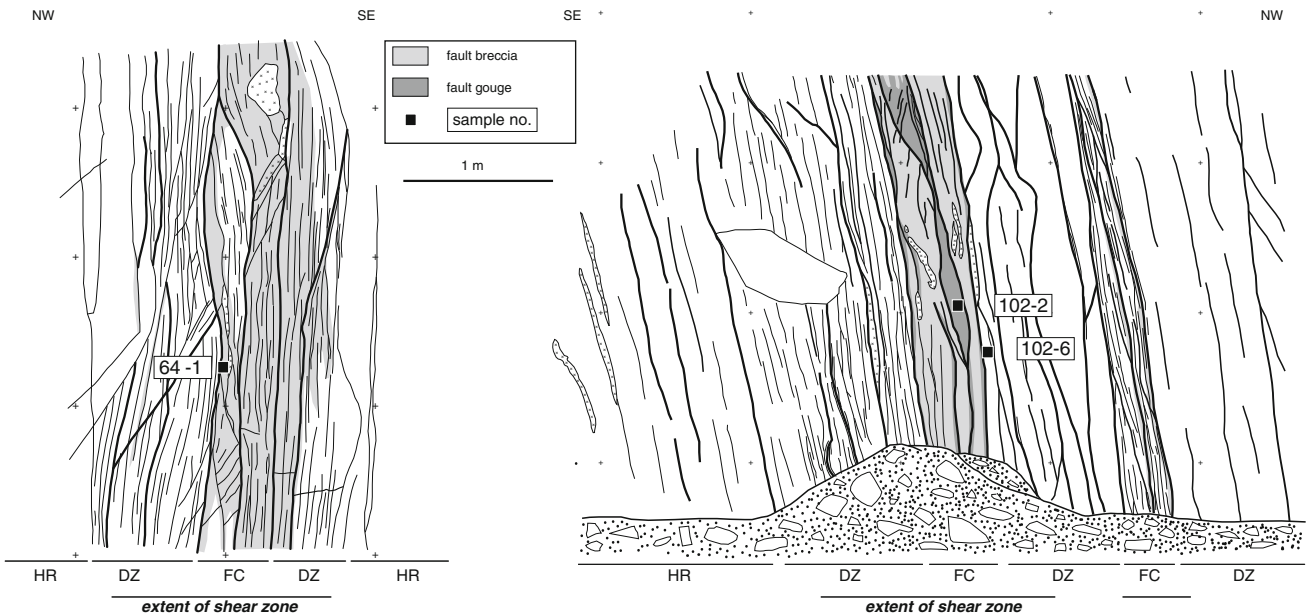

Fig. 9 Field records of faults F64 and F102, crosses indicate 1 m-grid scale. *Lines* represent fractures, *bold lines* main fractures. *Light grey colours* represent soft material (mainly cataclasite), *dark grey* material represents fault gouge material. The *light grey* area of fault F102 on the *left* corresponds with a mafic dike. Sample locations for X-ray diffractometry (Table 1) and *thin sections* (Plates) are indicated by *black squares*. *HR* host rock, *DZ* damage zone, *FC* fault core. Other samples mentioned in the text referring to the faults shown here and in the subsequent figures were taken from the opposite tunnel wall

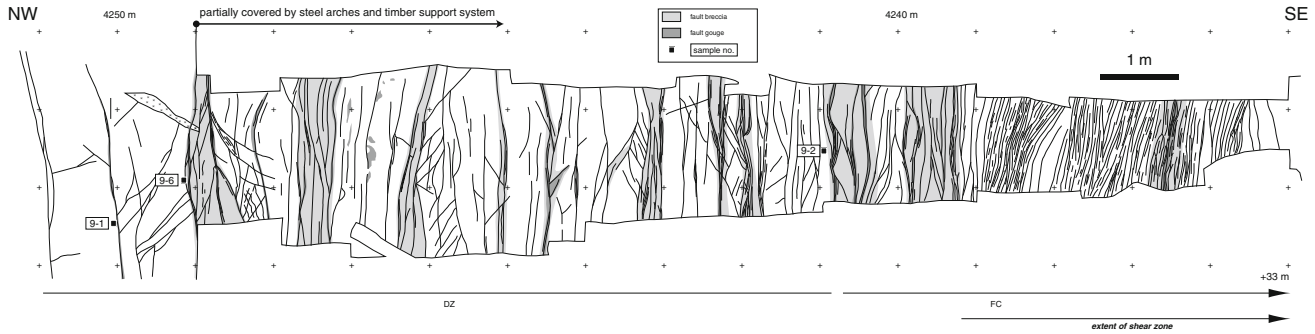

Fig. 10 Field record of fault zone F9. Total width of the fault zone l = 43 m. Figure is scaled to 75% compared to Figs. 9, 10 and 11. See Fig. 9 for legend

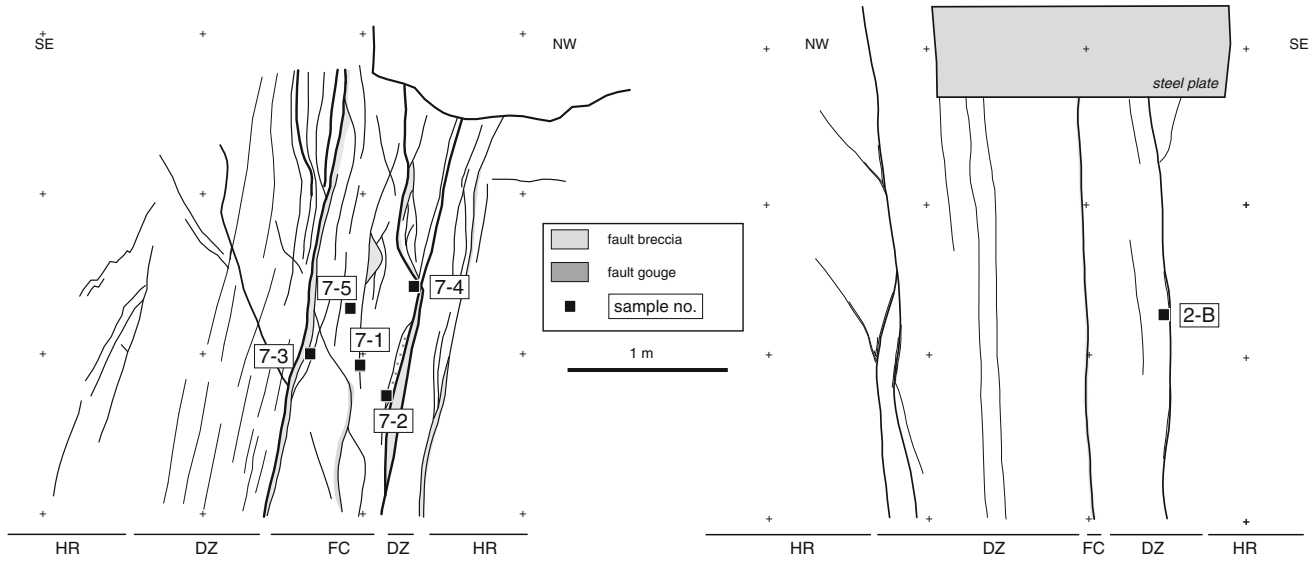

Fig. 11 Field record of faults F7 and F2. See Fig. 9 for legend

central fault core, and appearing entirely like a damage zone (22% of all analysed faults). Thin layers of fault gouge or fault breccia may be present as fracture fillings of cm width in major persistent fractures (example Fig. 11).

B. Fault developed in essentially undeformed granite composed of an intensely fractured and altered crush breccia and fault breccia of 1–2 m width (2% of analysed faults). This type of fault zones represents a fault core with only weakly developed damage zone. Main fractures may contain a few mm of gouge material. The cataclasite adjoining main fractures which enclose the fault core appears to be intact at first glance, but can be crushed by hand (example Fig. 12).

5 Microstructures and mineralogy of fault rocks in the Rotondo granite

5.1 Microfabric of fault rocks

The descriptive classification of fault rocks discussed above (Scholz 1990) is basically a macroscopic concept but can also be applied on to the millimetre-/thin section-scale. Note that no absolute criterion regarding size is given to distinguish rock fragments from the surrounding fine grained matrix.

Thin sections of 30 μm thickness of rock samples from fault zones mapped in Fig. 3 exhibit various microstructures as shown below. The focus is on fine grained fault rock.

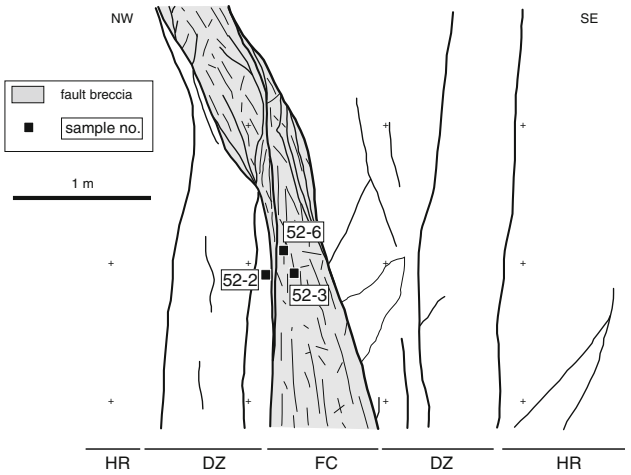

Fig. 12 Field record of fault F52. See Fig. 9 for legend

5.1.1 *Cataclasites*

Protocataclasites and cataclasites of the Bedretto tunnel are characterised by fracturing and fragmentation of the primary fabric and minor dislocation of the fragments (Fig. 4). On the scale of a few centimetres cataclasites often show networks of anastomosing micro-faults consisting of thin bands of fault breccia or fine grained gouge material.

5.1.2 *Fault breccia*

Fault breccias of the Bedretto tunnel show the abundance of more intensely fractured angular to edge-rounded clasts (Figs. 13, 14). Rock and mineral fragments (or clasts, respectively) may be entirely surrounded by fine grained gouge material, so that the fabric may then become partially matrix supported. Slightly dislocated fragments may show an offset to neighbouring fragments (Fig. 13a). Fault breccias occasionally show a foliation (Fig. 14c, d), where arrays of thin bands or finely dispersed and occasionally kinked mica define the foliation.

5.1.3 *Fault gouges*

Essentlially cohesionless fault gouges (Fig. 14 and partially Figs. 13b, c, 15b, 16) show matrix supported fabrics with subangular fragments. Fragment sizes are mostly between approximately 0.05 and 0.2 mm. However, some fault gouges show hardly any mica nor any foliation.

5.1.4 *Domains of fractured quartz grains*

In some thin sections from quartz-rich fracture-infillings sampled in faults F7, F9 and F88 domains of fractured quartz up to a few centimetres thickness (Fig. 17) have been

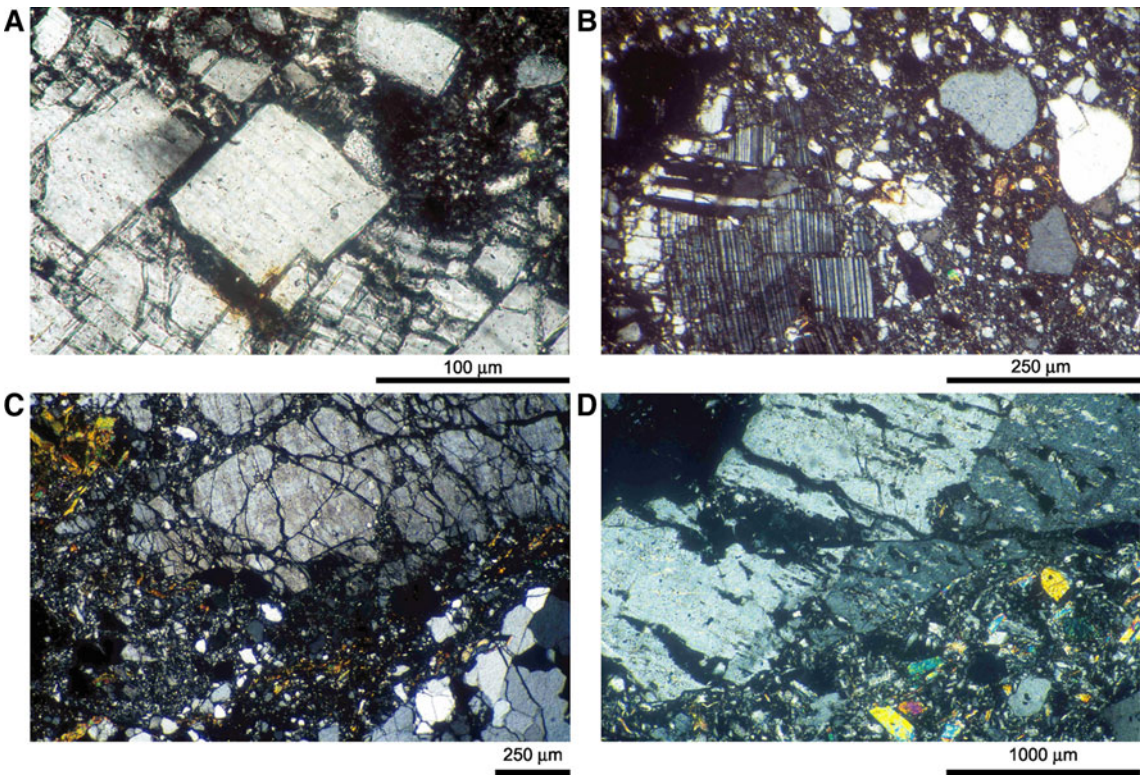

Fig. 13 Fault breccia showing larger fragments of feldspars and adjacent fine grained fault gouge material. Larger quartz grains appear to be rounded. **a–c** F7-1, **d** Microfault in twinned feldspar F9-2. *Crossed nicols*

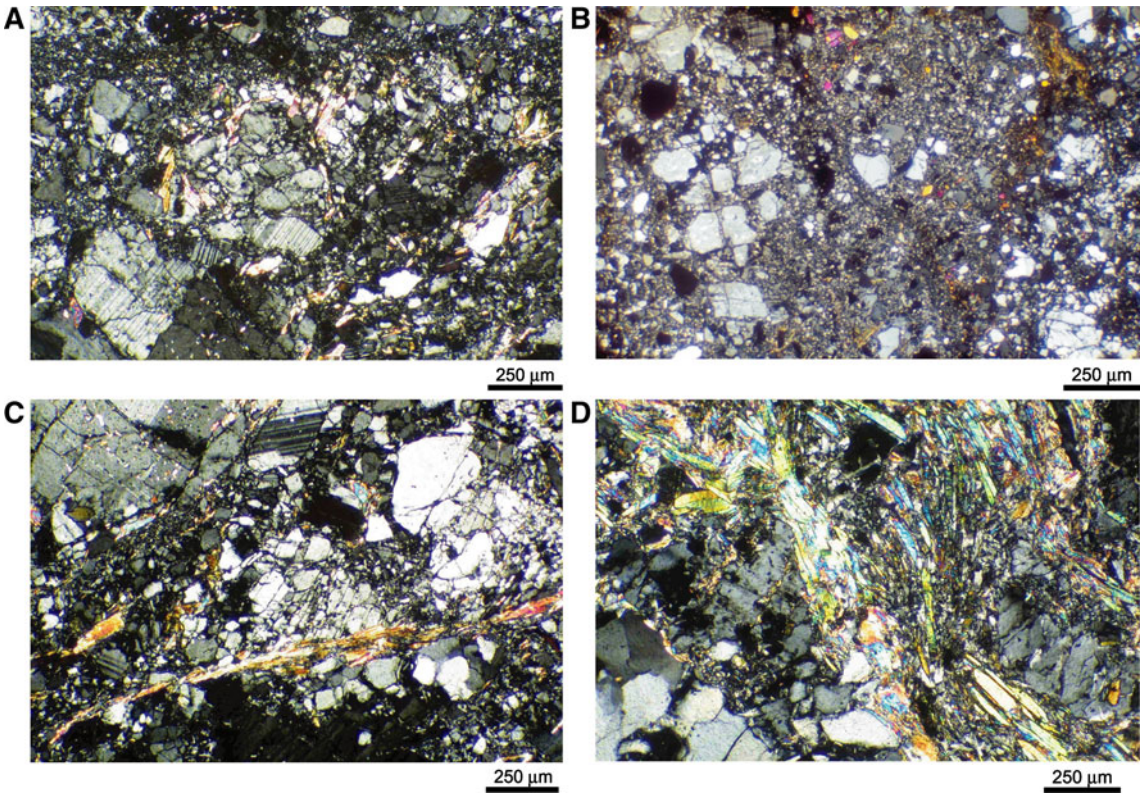

Fig. 14 Fine grained gouge material. **b** shows corroded quartz grains. **a**, **c** F7-5, **b** F7-1, **d** F9-3. *Crossed nicols*

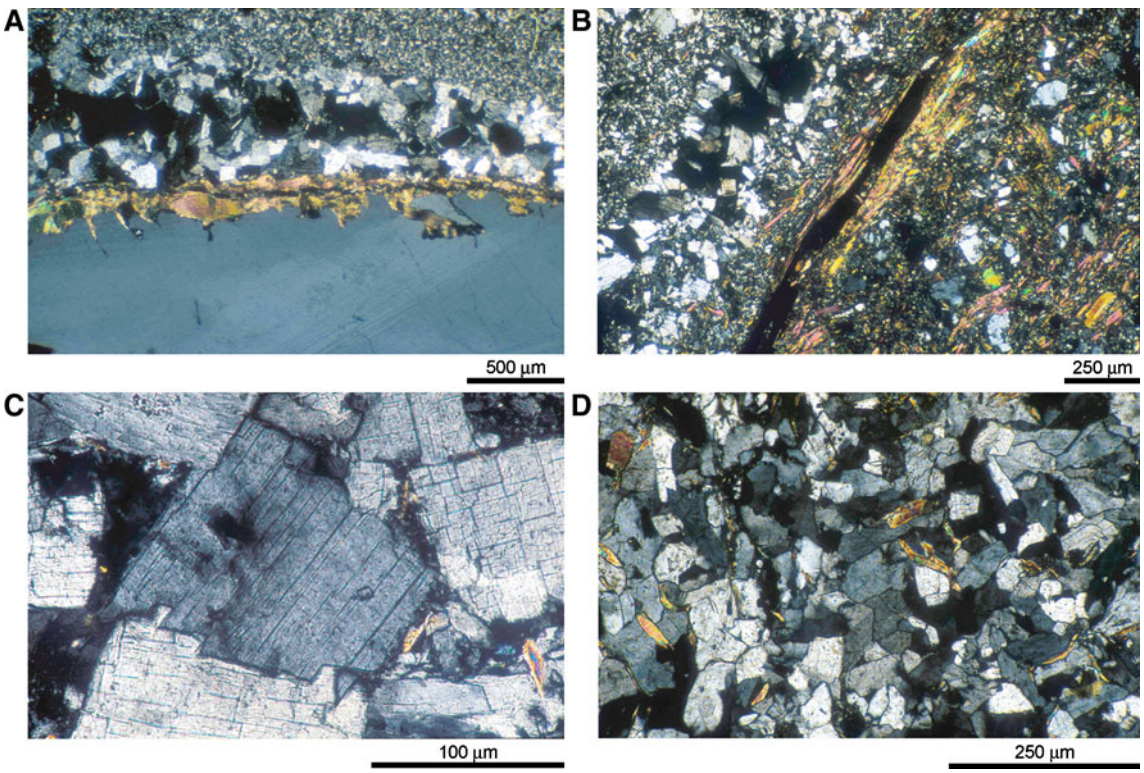

Fig. 15 Open fractures partially filled by laumontite. **a**, **b** F9-2, **c** F9-3, **d** F7-3. *Crossed nicols*

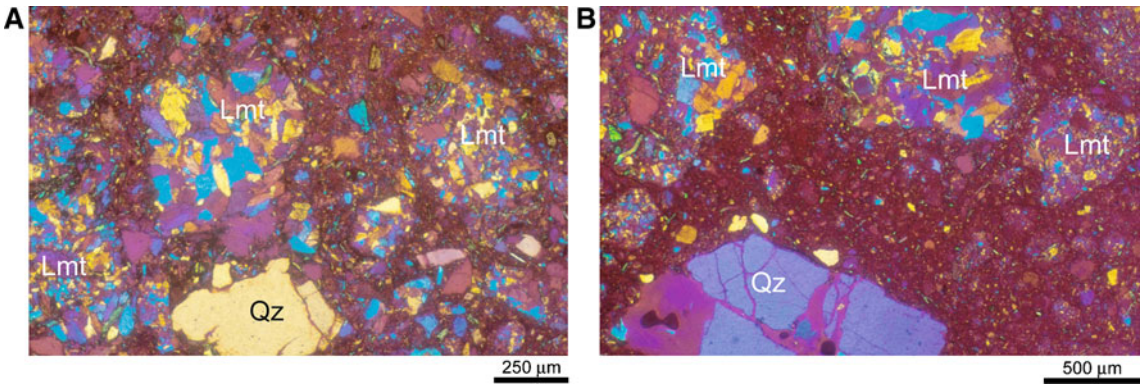

Fig. 16 Intraclasts of laumontite. **a**, **b** F9-3. *Crossed nicols* and compensator

observed. These domains neither show any regular nor any persistent fracture pattern or preferential fabric. The assignment to the classification of fault rock (Scholz 1990) is problematic, because no simple relation to the host rock can be established. The diameter of the individual grains is in most cases between 0.2 and 1.5 mm and represents a more or less equigranular (Passchier and Trouw 2005) fabric. The grain boundaries of quartz abundantly show irregular bulges like curved lobes and recesses (Figs. 15a, 17a–d). In few cases microfractures in quartz grains as mentioned above seem to have promoted the development of recesses, but typically these recesses developed without any optically observable fracture. According aggregates of quartz grains showing these typical recesses have occasionally also been observed as clasts in cataclasites (e.g. Fig. 14b) showing that this material was at least occasionally incorporated in cataclastic flow processes.

The compensator of the microscope shows that some quartz fragments in these domains have the same crystallographic and optical orientation (Fig. 17b). These quartz grains do not exhibit any evidence for mechanical deformation except for few minor microfractures (more like gaps) without any visible displacement. They also show hardly any indications for undulose extinction, whereas this feature is prevalent in the host rock as well as in most of the analysed brittle fault rocks of the Bedretto tunnel.

The space between these quartz fragments is filled with fine grained zeolite minerals, microscopically identified mainly as laumontite (Lmt) and to a lesser extent also as stilbite (Stb), respectively (Fig. 17), see also XRD-analyses below). These minerals enclose almost every quartz grain; only at few edges the quartz grains may touch one another. Very few biotites and sporadically other accessory minerals can be found between the quartz fragments.

5.2 Mineralogy of fault rocks and mineral reactions

The following alterations, mineral reactions and precipitates have been observed in fault breccias and fault gouges: reaction of biotite to chlorite, bleaching of biotite, sericitization and corrosion of feldspars, corrosion of quartz, precipitation of albite, zeolites, carbonate (calcite) and pyrite, respectively. In the undeformed protolith hardly any alteration reactions could be observed except for sericitization of feldspars and the retrograde alteration of accessory amphiboles.

5.2.1 Biotite–chlorite

In few cases a limited reaction of biotite to chlorite was observed as an incomplete retrograde reaction parallel to basal lattice planes. Chlorites in the Rotondo granite have blue-green to yellowish green pleochroism colours and irregular dark-purple interference colours. These optical characteristics suggest the presence of Fe^{II}-rich MgFe-chlorites (Tröger et al. 1982). The ratio of biotite to chlorite is large in fault rocks of the Bedretto tunnel, and chlorites show only small crystals. Biotites abundantly show bleached grain boundaries.

5.2.2 Alteration and corrosion of feldspars

Alkali feldspars generally show finely dispersed sericite. Feldspars in cataclasite and fault gouge commonly show a turbid appearance with slightly brownish colours in transmitted light. Albites as well as alkali feldspars show indications of orientation-preferred solution along crystallographically determined planes (Fig. 18). This secondary porosity is in most cases almost entirely filled by zeolites and to a lesser extent by secondary carbonate. This corrosion has in some cases lead to the formation of sceleton-like feldspars (Fig. 18).

5.2.3 Zeolites

Laumontite ($CaAl_2Si_4O_{12} \times 4\ H_2O$, Lmt) and stilbite ($NaCa_2Al_5Si_{13}O_{36} \times 14H_2O$, Stb) are the most eye-catching precipitates in secondary pore spaces of fault rocks of the

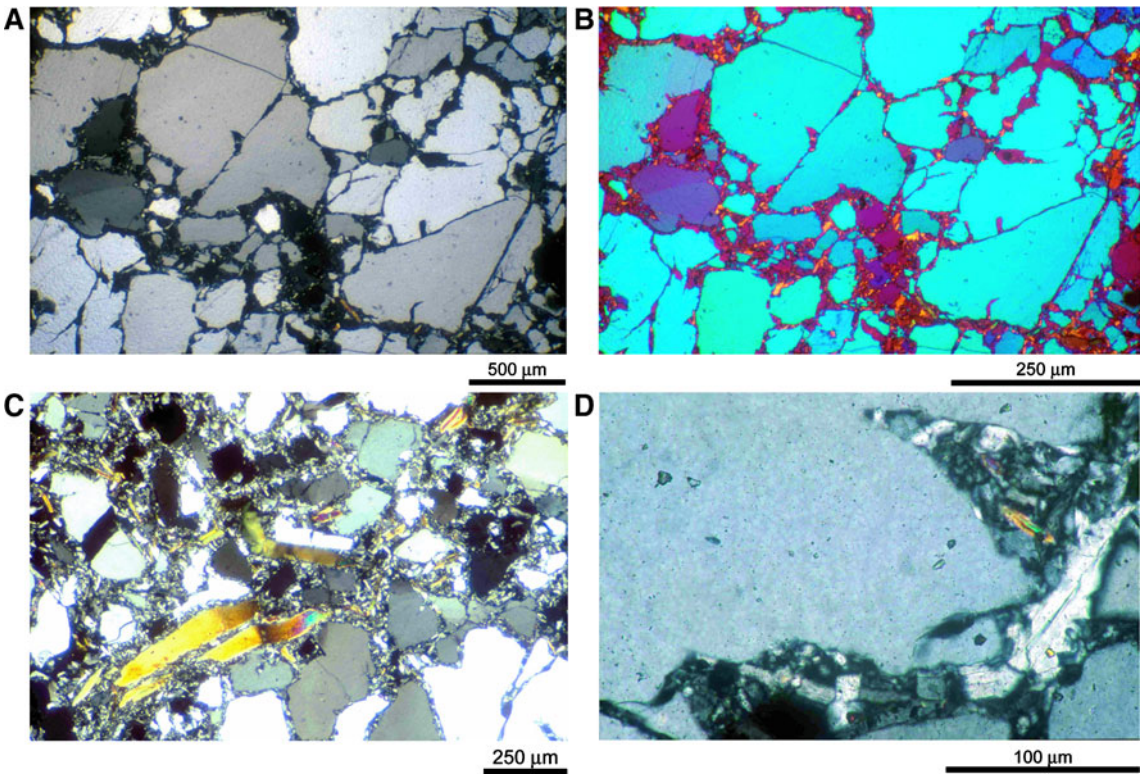

Fig. 17 Hydrothermal breccia showing quartz grains surrounded mainly by laumontite. **a–d** F88-3. **b** is a cutout of **a**. *Crossed nicols*, **b** additionally with compensator

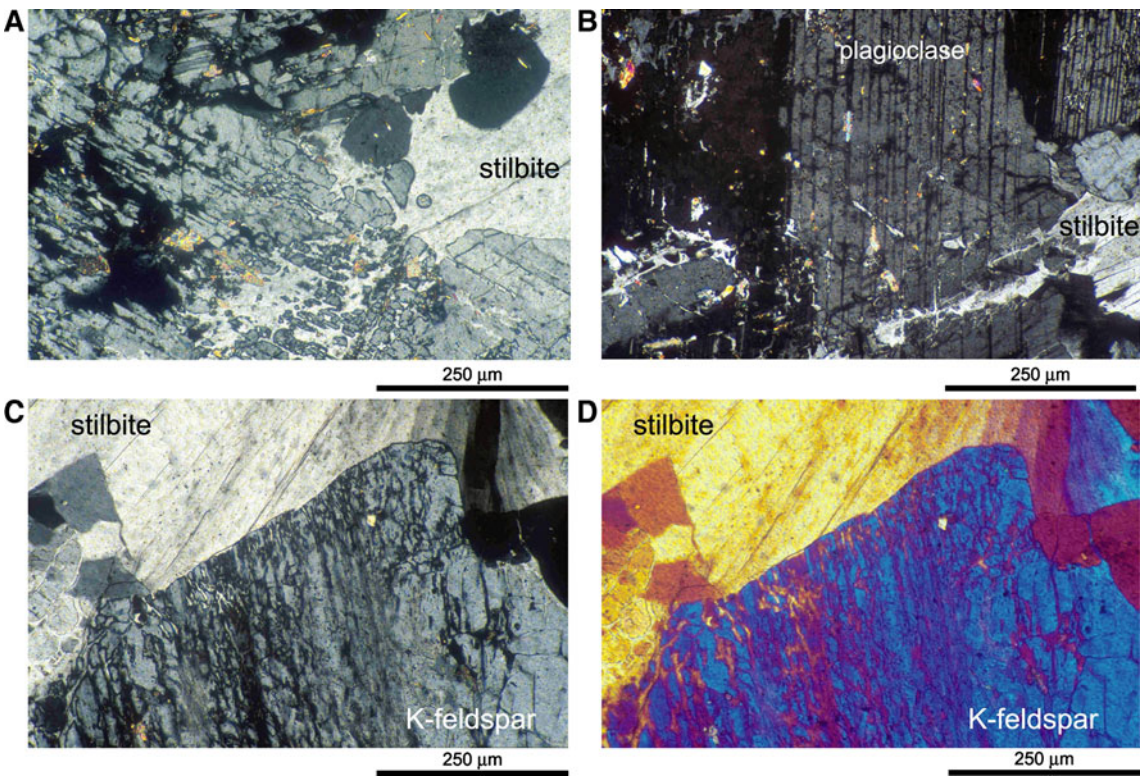

Fig. 18 Feldspars preferentially corroded along crystallographic directions. Pore spaces are filled by large crystals of stilbite. **a**, **b** F9-1, **c**, **d** F88. *Crossed nicols*, **d** additionally with compensator

Table 1 Semi-quantitative results of XRD-data of samples from fault zones in the Rotondo granite

Sample	Description	Tkm from south	qtz	akf	ab	ms	bt	mnt	lmt	stb	chl
Fault zones in brittle-ductile shear zones											
F67-2	fault breccia	4,614	+	o	−	o	o	++	+	− −	+
F102-2	fault gouge	4,629	++	o	− −	o	o	++	x	o	o
F64-1 A	fault gouge	4,670	o	+	o	o	o	o	++	x	−
F64-1 B	fault gouge	4,670	o	+	o	o	o	o	++	x	−
F64 SW	fault gouge	4,670	+	o	−	−	−	+	++	x	− −
F59 SW	fault gouge	4,770	+	+	+	o	o	++	− −	− −	− −
F46-1	fault gouge	4,968	++	o	− −	−	−	−	o	x	x
F46-2	fault gouge	4,969	++	o	o	−	−	+	− −	− −	o
Fault zones largely lacking ductile features											
F9-10A	fault breccia, qtz-vein	4,196	++	o	−	−	− −	x	+	x	x
F9-10B	fault breccia, qtz-vein	4,197	++	o	−	− −	−	− −	+	x	− −
F9-9A	fault breccia, qtz-vein	4,198	++	+	+	o	−	x	x	x	x
F9-9B	fault breccia, qtz-vein	4,199	++	+	+	−	−	x	x	− −	x
F9-2	fault breccia	4,248	++	o	−	−	− −	x	++	x	x
F9-6B	fault breccia	4,249	++	+	o	− −	− −	x	−	− −	x
F9-6C	fault breccia	4,249	++	+	o	−	−	− −	+	−	− −
F9-6D	fault breccia	4,249	++	+	o	−	−	− −	− −	o	− −
F88 A	fault breccia	4,257	o	++	−	o	− −	−	− −	++	− −
F88 B	fault breccia	4,257	o	++	−	o	− −	−	− −	++	− −
F7-1A	fault breccia	4,489	++	o	− −	−	−	x	o	− −	− −
F7-2	fault breccia	4,490	+	−	− −	− −	− −	x	++	x	x
F7-3A	fault breccia	4,491	+	−	− −	−	o	− −	++	x	− −
F7-3B	fault breccia	4,492	+	−	− −	− −	o	− −	++	x	−
F7-4A	fault breccia	4,493	++	− −	− −	− −	−	x	+	x	x
F7-5A	fault breccia	4,494	++	+	o	−	−	x	−	x	− −
F7-5D	fault breccia	4,495	++	++	+	−	−	− −	o	x	− −
F2-B	cataclasite.	4,998	++	+	+	o	−	− −	x	x	−
F52-3A	fault breccia & f.g.	4,849	++	+	o	−	−	−	−	− −	−
F52-3B	fault breccia & f.g.	4,849	++	+	−	−	−	− −	−	o	− −
F52-2	cataclasite	4,849	++	+	o	x	− −	o	− −	x	x
F52-6B	fault breccia & f.g.	4,849	++	o	o	− −	− −	o	− −	x	x
F52-6C	fault breccia & f.g.	4,849	++	+	+	−	− −	−	− −	x	− −

See Fig. 3 for location of fault zones. The locations of samples indicated in bold letters are shown in detail in Figs. 9, 10, 11, 12. The upper case letters of the sample numbers (A–D) refer to different samples prepared from the same hand specimen

Ap aplite, *f.g.* fault gouge, *qtz* quartz, *akf* alkali feldspars, *ab* albite, *mus* muscovite, *bt* biotite, *mnt* montmorillonite, *lmt* laumontite, *stb* stilbite, *chl* chlorite (clinochlore)

++, massive; +, main component; o, abundant; −, minor component; − −, traces; x, not detected

Bedretto tunnel. Important distinguishing features are the extinction angles (Lmt: $Z\Lambda c = 8°–33°$; Stb: $X\Lambda c = 5°$), the cleavage (Lmt: 3 main systems; Stb: 1) and the optical elongation (Lmt: always +; Stb: + or −). The presence of laumontite and stilbite has been verified by XRD-measurements (Table 1; Fig. 19).

Laumontite is widely abundant in thin sections of the analysed faults F7, F9, F52 (Figs. 3, 10, 11, 12) and F88. Domains of nicely developed equigranular, polygonal (Moore 1970) and interlocking mosaics of laumontites sometimes cover more than 80% of the entire thin section (Fig. 15c, d). In most cases no preferred crystallographic orientation of laumontite has been observed. In parts of these laumontite-rich domains elongated pore spaces remained open (Fig. 15a, b). Their inner surfaces are overgrown with large euhedral laumontite crystals clearly exceeding in grain size the surrounding laumontites. However, in case of very small crystals in fine fractures or in fine grained matrix the determination of the present mineral and and/or the unequivocal optical distinction between Lmt and Stb is difficult.

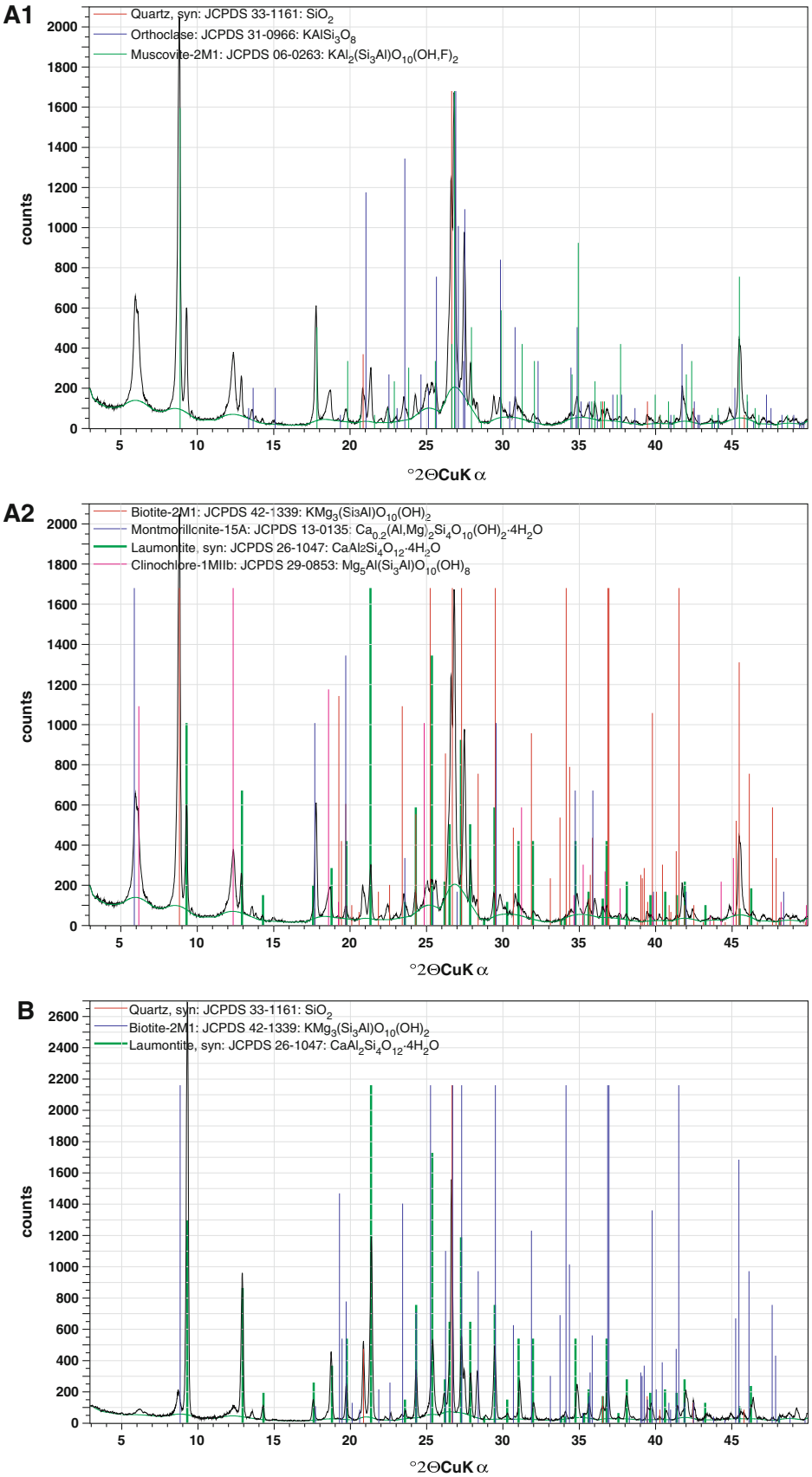

Fig. 19 XR-Diffractograms measured with a Scintag XDS 2000 (wave length: 1.5406 Å Cu Kα1). In **a1** the reference peaks for quartz, Alkali feldspar (orthoclase) and muscovite are shown for the X-ray diffractogram of sample F67-2. **a2** Reference *peaks* for biotite, montmorillonite, laumontite and chlinochlore (chlorite). **b** Reference peaks for quartz, biotite and laumontite in the diffractogram of sample F7-3

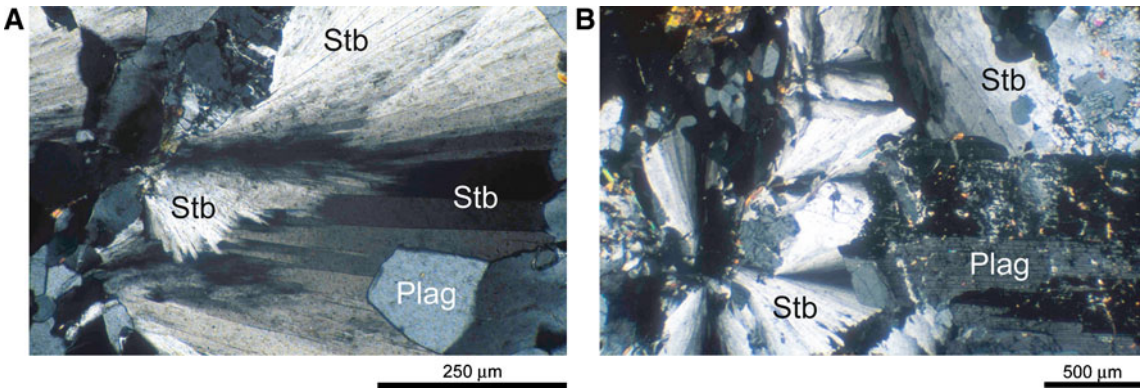

Fig. 20 Large stilbite crystals filling pore spaces of corroded fault rock. **a**, **b** F9-1. *Crossed nicols*

In some cases large stilbite precipitated in large pore spaces as anhedral globular or wedge-shaped aggregates up to 5 mm in diameter (Fig. 18). Feldspars corroded preferentially along crystallographic directions are filled by the same large pore space filling anhedral stilbite (e.g. in Fig. 18c, d). In samples of F52 (Figs. 3, 12) open fractures in cataclasite show euhedral stilbites of few millimetres length (Fig. 20). Slightly bent and fractured stilbite crystals may occasionally be present in such fractures, but apart from very few exceptions, pore-filling euhedral laumontites and stilbites do not show any indication of brittle deformation.

Laumontite and stilbite are also present in the matrix and as microfracture-filling minerals in fault breccias, cataclasites and gouge material (see XRD-analysis below). Furthermore, in some cataclasites and fault gouges rounded clasts of laumontite aggregates have been identified (Fig. 16). Minerals within these aggregates show considerably larger grain sizes than those within the surrounding gouge material.

5.2.4 Carbonates and epidote

Ca-Carbonate is abundant as subhedral pore-filling mineral and also within the matrix of fault gouges and fault breccia. It occurs in all structural types of fault rocks and host rock. In few thin sections carbonate precipitated in large open pores spaces along fractures. The relation to adjacent stilbites neither shows any clear succession of growth nor clear indications for simultaneous growth.

Probably authigenic epidote/clinozoisite appears predominantly in cataclasites as accumulated clasts, but it could not be clarified, whether they represent reaction products or primary minerals of the host rock. Euhedral rectangular opaque pyrite in some fine grained cataclasites does not show any indication of alteration.

5.2.5 X-ray diffractometry

In order to identify the mineralogy of fault rocks most of the samples used for thin section analysis were also analysed using a Scintag XDS 2000 X-ray diffractometer. The following minerals could be identified in most of the 31 samples: quartz, alkali feldspar (orthoclase), albite, white mica (muscovite), laumontite and biotite. Chlorite (clinochlore), Ca-montmorillonite, stilbite and calcite were identified only in few samples. The mineral contents were compared semi-quantitatively (Table 1).

Based on these results two different groups of typical mineralogical composition can be distinguished for fault rocks in the Bedretto tunnel: For the first group of brittle-ductile faults a high content of mica is characteristic as well as a moderate content of biotite and a variably high content of the corresponding low-temperature alteration products, like montmorillonite and chlorite (upper part of Table 1; see also Fig. 19, no further distinction of clay minerals was carried out). The content of zeolites is very variable, but traces were found in most cases. Laumontite is generally much more abundant than stilbite. In samples of the fault zone F64 laumontite represents even one of the main rock forming minerals.

The second group of brittle fault zones largely lacking structures of ductile shear zones (lower part of Table 1) shows in addition to feldspar and quartz only zeolites and Ca-carbonate. Samples of the fault zones F9 and F7 show high contents of laumontite, whereas the content of stilbite is low or could not be detected at all. In samples taken from F88 stilbite is abundant, whereas laumontite is lacking. The content of mica in all samples is low to moderate.

6 Discussion

6.1 Regional fault pattern

The orientations of fault zones observed at the surface and in the Bedretto tunnel differ from the fault pattern in the area of the Gotthard pass and east of it as mapped by Lützenkirchen (2002) and Zangerl et al. (2006). In the Gotthard pass area dikes, ductile shear zones as well as steeply dipping joints

served as nuclei for the formation of brittle fault zones (Zangerl et al. (2006). In the eastern Aar massif ductile shear zones dominate over brittle faults (Laws et al. 2003).

According to Steck (1968), Arnold (1970), Merz (1989), Marquer (1990), Lambert et al. (1992) und Pettke and Klaper (1992) ductile shear zones with steeply dipping mineral lineations in the Gotthard massif were formed in a NW–SE oriented compressional stress regime. There is no agreement in the literature whether these shear zones have to be attributed solely to Alpine and/or to Variscan compressional tectonics. The later formation of probably right-lateral brittle strike-slip (Zangerl et al. 2006) or oblique-slip faults observed in the Bedretto tunnel requires a different stress regime compared to Alpine NW–SE compressional tectonics.

6.2 Deformation mechanisms

By far most of the observed micro-structures in fault rocks of the Bedretto tunnel can clearly be attributed to cataclastic flow, including distributed microcracking (Figs. 4, 6, 13) and frictional sliding of the fragments (Fig. 13) and wear abrasion (Fig. 14), resulting in fault breccia, cataclasite and fault gouge with angular and rounded fragments showing a large variation in grain sizes. On the other hand the quartz-rich domains mentioned above (Fig. 17) show fractured equigranular grains and indications for intense corrosion, but almost no indication for cataclastic flow. The fabrics of these quartz-rich domains are interpreted as hydrothermal breccias (Jébrak 1997) formed by fluid-assisted brecciation and corrosive wear. Fluid-assisted brecciation can be divided into two steps: hydraulic fracturing and critical fracturing.

Hydraulic fracturing is supposed to be a common process in fault zones (Sibson 1977, 1986; Chester et al. 1993; Sibson 2000; Boullier et al. 2004b) and relates to an increase in fluid pressure leading to the decrease of effective stresses, promoting tensile fracturing or fracture propagation predominantly along preexisting planes of weakness. The increase of the fluid pressure may be due to a decrease in fault permeability (Sibson 2000), or may be due to boiling fluids as a result of geochemical reactions (Walder and Nur 1984; Parry and Bruhn 1990). Critical fracturing is related to a sudden drop in fluid pressure (e.g. from hydraulic fracturing and porosity increase) and the subsequent loss of equilibrium between regional stress and fluid pressure (Hobbs 1995). Decompression of the fracture walls will lead to spalling instabilities and the formation of "implosion breccias", especially in dilatational jogs (Sibson 1986; Jébrak 1997).

After Jébrak (1997) both types of fluid-assisted brecciation generate in situ fragmentation fabrics in a jigsaw puzzle pattern without significant rotation of the fragments (Fig. 17a, b). The absence of fragment rotation indicates limited frictional shearing during brecciation. Fluid assisted breccias preferentially follow preexisting discontinuities and are commonly found in extensional regimes with high dilation ratios (Jébrak 1992). Frequently they show mineralogically simple infillings lacking banding due to rapid mineral precipitation. The grains are usually of similar size (Jébrak 1992). All these features are documented in Fig. 14a–c.

Corrosive wear (Stachowiak and Batchelor 1993; Jébrak 1997) may occur under chemical disequilibrium between fluid and rock, leading to breccia composed of chemically altered fragments showing hardly any reorientation. Figure 17d shows very irregular dissolution of quartz grain boundaries which might be the result of chemical wear. The fact that biotite is present in some corrosion gaps may indicate, that corrosive wear initiated at temperatures exceeding 300°C (see below).

Fluid-assisted brecciation, especially critical fracturing, can be regarded as common process during faulting (Sibson 1992; Byerlee 1993; Chester et al. 1993; Robert and Boullier 1994; Miller et al. 1996; Hardebeck and Hauksson 1999). In by far most cases these microstructures will be destroyed in subsequent mechanical deformation processes during recurrent fault activity (e.g. Sibson 1992). In permeable subsidiary fractures of damage zones microstructures associated with hydraulic fracturing are most likely to be preserved. Such well developed breccias have been found in the damage zones of fault zones F7, F9 and F88.

6.3 Temperature and depth constraints for brittle faulting

In contrast to metamorphic environments and closed systems in the laboratory, natural hydrothermal environments in fault systems of the upper crust have to be considered open systems, at least partially or temporarily (Bruhn et al. 1994). Secondary mineral assemblages in voids and fractures are dependent on pressure, temperature and fluid chemistry. The effect of mass transport by fluids, variable fluid chemistry and recurrent sudden pressure changes on minerals may be considerable and complicates an assessment of *P–T*-conditions based on observable mineral reactions and assemblages. Additionally, some minerals typically formed under hydrothermal conditions (approximately 350–100°C) occur in a wide range of *P–T* conditions. Their occurrence may consequently be not diagnostic (Henley and Ellis 1983).

Hydrothermal reactions are largely restricted to the immediate vicinity of permeable structures and interconnected pore spaces. The complete chemical equilibrium will not be entirely achieved for the adjacent matrix rock

due to the inertia of mineral reactions at low temperatures (Spear 1993). Nevertheless, the analysis of observed fault structures and mineral assemblages of fault rocks in the Bedretto tunnel allows to bracket the temperatures prevailed during brittle deformation processes and to establish a model for the fault zone development in the Rotondo granite.

6.3.1 *Quartzo-feldspathic minerals in fault rocks*

Few indications of chemical alteration of feldspars in intensely deformed fault gouge (sericitisation) suggest that feldspars were relatively stable during brittle faulting, except for the cases discussed below. Feldspars as alteration products in geothermal environments as well as in brittle fault zones have been observed on a relatively wide range of temperatures in active geothermal systems (e.g. Anderson et al. 1983; Henley and Ellis 1983). Albite may form at temperatures above approximately 130°C as dewatering product of analcime + quartz (experimental data after Thompson (1971); Fig. 21).

Fine grained quartz is abundant in the matrix of fault rock. Quartz-rich veins have been identified in few cases (F7, F9 and F88), where quartz forms large grains which were later affected by hydrothermal brecciation, presumably chemical corrosion and fluid-assisted brecciation. Quartz is stable over a wide range of temperatures above approximately 120°C (Henley and Ellis 1983). For temperatures below 300°C detritial quartz is relatively inert to hydrothermal fluids (Hoagland and Elders 1978).

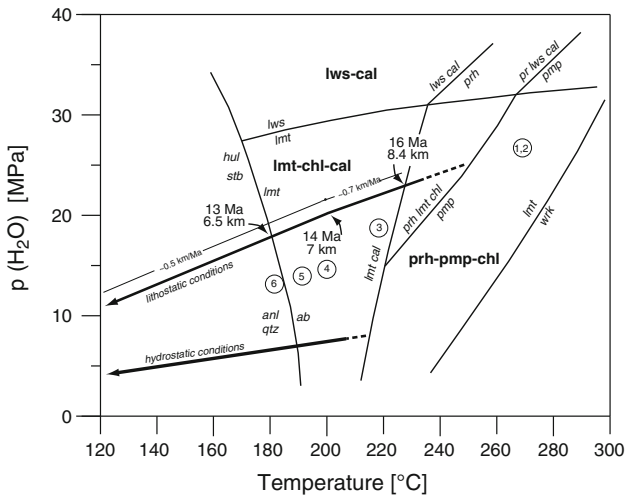

Fig. 21 *P–T* diagram for laumontite and reaction products in the ACF-system [after Liou (1971a, b, c, d), Thompson (1970, 1971), and Cho et al. (1987)]. Abbreviations according to Kretz (1983): *hul* (heulandite), *stb* (stilbite), *anl* (analcime), *qtz* (quartz), *lmt* (laumontite), *ab* (albite), *lws* (lawsonite, *cal* (calcite), *chl* (chlorite), *prh* (prehnite), *pmp* (pumpellyite), *wrk* (wairakite). The postulated *P–T*-evolution for the Rotondo granite in the Bedretto tunnel is shown. *Numbers* refer to the hypothetical *P–T* model in chapter 6.3.4

Biotite showing bleached grain boundaries and in some cases transformations to chlorite indicates limited alteration processes. Biotite is stable at temperatures above approximately 325°C (Henley and Ellis 1983). Chlorite is stable in different crystallographic configurations above 130°C (Henley and Ellis 1983) up to lower greenschist metamorphic conditions. However, biotite showing alteration to chlorite was comparatively rare in the analysed thin sections, suggesting this retrograde reaction may be not diagnostic in this case.

Intense corrosion of feldspars and quartz was almost exclusively observed in association with hydrothermal breccias. In some of the corrosion recesses of quartz grains, biotite as new formed minerals has been observed. Consequently, temperatures were probably slightly above 300°C during the onset of hydrothermal brecciation and subsequent chemical corrosion.

6.3.2 *Zeolites in fault rocks*

Zeolites have been observed, among other environments, in fault zones (e.g. Anderson et al. 1983; James and Silver 1988; Chester et al. 1993; Bruhn 1994; Boullier et al. 2004a; Matsuda et al. 2004; Pennacchioni et al. 2006; Zangerl et al. 2006; Tanaka et al. 2007) as well as in hydrothermally active regions (Coombs et al. 1959; Utada 1965; Seki et al. 1969; Henley and Ellis 1983; James and Silver 1988; Chipera and Apps 2001). Vincent and Ehlig (1988) observed laumontite minerals in veins associated with fractures in granitic rocks and gneisses north of the San Andreas fault. It occurs as replacement of anorthite component of plagioclase. Tanaka et al. (2007) have determined temperatures of 130–200°C present during the formation of ultracataclasites associated with zeolite precipitation in depths of 4–8 km the Nojima fault (Japan). Anderson et al. (1983) observed finely dispersed as well as vein-type laumontite together with analcime, mordenite and chlorite in cataclastic fault rock of primary granitoid composition. Apart from analcime, which has not been found in this study nor by Kipfer and Stuker (1979), the mineralogy of these fault rocks sampled from in outcrops of the San Gabriel fault in California widely resembles that found in the Bedretto tunnel.

Conditions of reaction isograde of zeolites have been determined experimentally (Campbell and Fyfe 1965; Thompson 1970; Liou 1971b, c, d; Thompson 1971; Cho et al. 1987). However, constraints like pH, fluid pressure, pCO_2, H_2S-activity and chemical composition of water and steam, respectively, are crucial for the thermodynamic equilibrium conditions, but are virtually unknown for natural fossil hydrothermal systems. Therefore, the comparison of experimentally derived data and natural systems has to be conducted with care.

In the Bedretto tunnel, laumontite is the key mineral for the assessment of *P–T*-conditions during faulting. The reaction isograde for zeolites and reaction products are shown in the *P–T*-diagram of Fig. 21. In a system H_2O–$Ca_{1/3}$–$Al_{2/3}O_{4/3}$–SiO_2 the assemblage laumontite-albite-carbonate is stable between approximately 190–210°C for $P_{(fluid)}$ lower than 10 MPa; for $P_{(fluid)} = 27$ MPa the limit ranges between 170 and 225°C. At higher temperatures laumontite dewaters to wairakite + $2H_2O$. This isograde is strongly pressure-dependant (after Liou (1971b); 5 MPa: ca. 240°C; 30 MPa: ca. 300°C). Pumpellyite, prehnite or wairakite ($CaAl_2Si_4O_{12}{\cdot}2H_2O$), being stable at higher temperatures and pressures, have neither been found by Kipfer and Stuker (1979) nor by own investigations of thin sections and XRD-analyses of samples from the Bedretto tunnel. This applies also for analcime, which indicated temperatures lower than 170/190°C (Liou 1971b).

Stilbite as second abundant zeolite often occurs together with heulandite in natural systems, defining for instance the low zeolite facies of Seki et al. (1969), whereas laumontite frequently coexists with wairakite, being diagnostic for a 'high zeolite facies'. Figure 21 shows that in the system H_2O-$Ca_{1/3}$-$Al_{2/3}O_{4/3}$-SiO_2 stilbite is not stable in presence of laumontite, though they may coexist in certain environments due to incomplete reactions or poor permeability (Ohtani et al. 2000; Matsuda et al. 2004; Pennacchioni et al. 2006). In fact in the thin sections no coexistence of laumontite and stilbite has been observed. The XRD measurements presented in Table 1 in show only traces of one mineral in cases where the other is present in considerable amounts.

Samples of fault rock of the Bedretto tunnel show rock fragments or aggregates consisting of laumontite, which were incorporated as clasts in cataclasites (Fig. 16) and fault gouges. This indicates recurrent fault activity, where events of fault slip are succeeded by phases of precipitation of laumontite, which again were comminuted. Large euhedral laumontite abundant in fractures and veins which obviously has been spared from deformation suggests, that faulting processes must have decreased considerably or almost ceased before the temperature dropped below approximately 180°C (Fig. 21). These euhedral laumontites thus represent in part post-deformation precipitates. Laumontite possibly also precipitated in open fractures before the onset of brittle faulting; thus it cannot be used for the determination of *P–T*-conditions present at this stage. Furthermore it is also possible that the coplanar zeolite wairakite may have formed in an early stage of faulting and later underwent a dewatering reaction to laumontite. Euhedral stilbite is most certainly formed exclusively during a post-deformation phase, since it does not show any indication of deformation. It represents the latest zeolite mineral which precipitated under retrograde conditions from fluids at temperatures below 190°C.

Kipfer and Stuker (1979) found scolecite, laumontite, heulandite and stilbite on joint surfaces in the southern part of the Bedretto tunnel (Tm 1,140–3,000), whereas in the northern part, where the samples described above were taken, only the occurrence of stilbite, and at one location also heulandite has been observed.

6.3.3 *Accessory minerals in fault rock*

As mentioned above, other minerals represent alteration products: Epidote has been observed in hydrothermal environments down to 220–200°C (Liou 1973) but could not be observed as authigenic mineral reaction from biotite. After Guilbert and Park (1986) the assemblage chlorite-epidote-K-feldspar is stable at temperatures around 250°C.

Pyrite is stable in a large range of temperature; its formation is basically dependant on the availability of Fe^{2+} and S^{-}. Large euhedral crystals were found in the Bedretto tunnel in a schistous zone between Tm 4,919–4,940 by Kipfer and Stuker (1979).

6.3.4 *Hypothetical P–T model*

As shown above, laumontite is stable at fluid pressures (P_{H2O}) below approximately 27–30 MPa (Fig. 21). For a closed system with pore pressures equal to lithostatic pressure and using a rock density of 2.7 g/cm^3 the maximum depth for the formation of laumontite is about 10–11 km. No minimum depths can be deduced for laumontite unless yugawaralite is present (Zeng and Liou 1982).

Glotzbach et al. (2010) studied the thermal and exhumation history of the Central Aar and Gotthard massifs based on apatite and zircon fission track and apatite (U-Th)/He data from samples taken along the Gotthard road and A2 tunnel transect. Based on these data and a paleogeothermal gradient of 25 K/km we estimate that the rocks of the Bedretto tunnel at 1,500 m asl crossed the 200°C isotherm (close to cessation of fault activity) about 14 Ma, and the 120°C-isotherm about 8 Ma ago. Glotzbach et al. (2010) document remarkably uniform uplift and erosion rates along the Gotthard A2 tunnel 10 km east of the Bedretto tunnel and conclude that vertical offsets along faults have been small (<0.6 km) since about 14 Ma, which is consistent with our findings. In addition they postulate hydrothermal activity after the cessation of deformations along selected faults in the Aar Massif (from local anomalies in apatite fission track ages), tentatively occurring at about 6 Ma. This is in contrast to the Tavetsch Massif or the southwestern Aar massif, where brittle deformations along faults are supposed to last substantially longer (Wyder and Mullis 1998; Persaud and Pfiffner 2004).

Based on the observations from the Bedretto tunnel, a geothermal gradient of 25 K/km, and the findings of Glotzbach et al. (2010) we postulate the following development of brittle faulting in the Rotondo granite (Fig. 21):

1. Corrosion of feldspars and quartz and formation of biotite in fractures in fault zones at temperatures below 300°C.
2. First occurrence of laumontite at ca. 10–11 km depth and approx. 280°C.
3. Recurrent strike-slip faulting between approximately 18 and 14 Ma, development of fault breccias, cataclasites and fault gouges. In some cases faulting was associated with (sudden) pressure changes and thus the formation of fluid-assisted breccias in damages zones. Potential drop of lithostatic fluid pressure to hydrostatic fluid pressure.
4. Cessation of strike-slip faulting at approximately at temperatures of ~200°C, 14 Ma and 7 km depth.
5. Mineralisation of euhedral laumontite in pore spaces. Further cooling and exhumation.
6. Mineralisation of euhedral stilbite in pore spaces. Further cooling and exhumation.

The actual seismicity within the Gotthard massif is notably low (Kastrup et al. 2004; Baer et al. 2005; Deichmann and Baer 2007) and might be explained by the cessation of significant tectonic fault movements as described above. Also the fault scarps running parallel to the SW–NE-trending Urseren and Tujetsch valleys (Jäckli 1951; Eckardt et al. 1983; Persaud and Pfiffner 2004; Ustaszewski et al. 2007; Ustaszewski and Pfiffner 2008) might not be of neotectonic origin but most probably represent post-glacial unloading and gravitational slope movements along pre-exiting tectonic faults.

7 Summary and conclusions

The Bedretto tunnel offers excellent insights into late Alpine stages of brittle faulting in a granitic environment. Faults and fault zones developed preferentially along preexisting NE–SW-oriented subvertical ductile shear zones and mafic dikes, paralleling the main foliation. Gently dipping slickenside striations on fracture surfaces suggest predominant strike-slip fault movements. Most faults and fault zones show a well developed fault core, where intense cataclasis lead to the formation of cataclasites, fault breccias and fault gouges. With few exceptions the thickness of gouge-filled fractures does not exceed a few centimetres. Damage zones adjacent to the fault core are characterised by fault breccias and cataclasite and are pervaded by dm-spaced prominent fractures. About 75% of the 79 faults and fault zones are located within the extent of preexisting ductile shear zones. 25% of brittle faults and fault zones developed in massive granite. More than 80% of the faults and fault zones do not exceed a width of 2 m.

Microfabrics of fault rocks show transitions from ductile shearing to brittle faulting under retrograde conditions. By far most of the observed micro-structures in brittle fault rocks of the Bedretto tunnel can clearly be attributed to distributed cataclastic deformation processes (cataclastic flow) such as fragmentation through microfracturing, sliding and rotation of fragments, resulting in cataclasite, fault breccia, and fault gouge with angular fragments showing a large variation in grain sizes. At some locations quartz filled fractures show special fabrics with domains of equigranular, irregularly shaped quartz grains of uniform optical orientation. This fabric can best be explained by hydraulic and critical fracturing, resulting from locally high fluid pressures during faulting. These fluid-assisted failures typically result in implosion breccias in dilatational jogs between mobilized shear fractures or in new tensile fractures (Sibson 1986; Jébrak 1997). In addition corrosive wear lead to chemical corrosion and dissolution of material at grain boundaries of quartz grains.

Only few retrograde reactions can be clearly identified in strongly deformed fault rocks (e.g. biotite->chlorite, sericitisation). In hydrothermal breccias intense corrosion of feldspars and quartz, together with the formation of biotite could correspond to the onset of brittle deformation at temperatures slightly above 300°C. Laumontite is common in fault rock of the Bedretto tunnel and is incorporated as clasts in cataclasites and fault gouge, indicating recurrent faulting activity at temperatures below 280°C. Equigranular, polygonal and interlocking mosaics of laumontite indicate significantly decreasing fault activity at ca. 200°C. Undeformed stilbite is present in previously open fractures and corroded feldspars and formed at temperatures below 170–190°C. Based on these fabrics and published fission track dates it is postulated that the main brittle faulting ceased about 14 Ma ago at a depth of about 7 km. Only minor slip events may have been accommodated since then, probably within low-cohesion fault gouges, which is in agreement with the low seismicity of today.

Acknowledgments The authors would like to thank the maintenance team of the Matterhorn-Gotthard-Bahn for providing access to the Bedretto tunnel trough the Furka -tunnel. Thanks also to Mrs. Bischof (ETH Zurich) for preparing the thin sections. In addition, we would like to thank Dr. Christian Zangerl and Dr. Ulrich Ofterdinger for numerous discussions and support during the work underground and the field mapping campaign. The reviewers Drs. Jussi Mattila and Paul Bossart provided many valuable comments, the authors would like to thank them as well.

References

Anderson, I. J., Osborne, R. H., & Palmer, D. F. (1983). Cataclastic rocks of the San Gabriel fault—An expression of deformation at deeper crustal levels in the San Andreas fault zones. *Tectonophysics, 98*, 209–251.

Arnold, A. (1970). Die Gesteine der Region Nalps-Curnera im nordöstlichen Gotthardmassiv, ihre Metamorphose und ihre Kalksilikalfels-Einschlüsse. Beiträge zur Geologischen Karte der Schweiz, N.F. 138.

Baer, M., Deichmann, N., Braunmiller, J., Husen, S., Fäh, D., Giardini, D., et al. (2005). Earthquakes in Switzerland and surrounding regions during 2004. *Eclogae Geologicae Helvetiae, 98*(3), 407–418.

Barton, C. A., Zoback, M. D., & Moos, D. (1995). Fluid flow along potentially active faults in crystalline rock. *Geology, 23*(8), 683–686.

Bernotat, W., & Bambauer, H. U. (1980). Die Mikroklin/Sanidin-Isograde in Aar- und Gotthardmassiv. *Eclogae Geologicae Helvetiae, 73*(2), 559–561.

Blenkinsop, T. (2000). Deformation microstructures and mechanisms in minerals and rocks. New York: Kluwer Academic.

Blenkinsop, T. G., & Sibson, R. H. (1992). Aseismic fracturing and cataclasis involving reaction softening within core material from the Cajon Pass drill hole. *Journal of Geophysical Research, 97*(B4), 5135–5144.

Boullier, A. M., Fujimoto, K., Ito, H., Ohtani, T., Keulen, N., Fabbri, O., et al. (2004a). Structural evolution of the Nojima fault (Awaji Island, Japan) revisited from the GSJ drill hole at Hirabayashi. *Earth, Planets, and Space, 56*(12), 1233–1240.

Boullier, A. M., Fujimoto, K., Ohtani, T., Roman-Ross, G., Lewin, É., Ito, H., et al. (2004b). Textural evidence for recent co-seismic circulation of fluids in the Nojima fault zone, Awaji island, Japan. *Tectonophysics, 378*(3–4), 165–181.

Brace, W. F. (1980). Permeabilty of crystalline and argillaceous rocks. *International Journal of Rock Mechanics and Mining Sciences, 17*, 241–251.

Bruhn, R. L. (1994). Fracturing in normal fault zones: Implications for fluid transport and fault stability. USGS open file report proceedings: The mechanical involvement of fluids in faults/94-228, 231–246.

Bruhn, R. L., Yonkee, W. E., & Parry, W. T. (1994). Fracturing and hydrothermal alteration in normal fault zones. *PAGEOPH, 142*, 609–644.

Buergi, C., Parriaux, A., Franciosi, G., & Rey, J.-P. (1999). Cataclastic rocks in underground structures—Terminology and impact on the feasibility of projects (initial results). *Engineering Geology, 51*(3), 225–235.

Byerlee, J. (1993). Model for episodic flow of high-pressure water in fault zones before earthquakes. *Geology, 21*, 303–306.

Caine, J. S., Evans, J. P., & Forster, C. B. (1996). Fault zone architecture and permeability structure. *Geology, 24*(11), 1025–1028.

Caine, J. S., & Forster, C. (1999). Fault zone architecture and fluid flow: insights from field data and numerical modeling. *Faults and subsurface fluid flow in the shallow crust, American Geophysical Union., 113*, 101–127.

Campbell, A. S., & Fyfe, W. S. (1965). Analcime-albite equilibria. *American Journal of Science, 263*, 807–816.

Chester, F. M., Evans, J. P., & Biegel, R. L. (1993). Internal structure and weakening mechanisms of the San Andreas fault. *Journal of Geophysical Research, 98*, 771–786.

Chester, F. M., Friedman, M., & Logan, J. M. (1985). Foliated Cataclasites. *Tectonophysics, 111*, 139–146.

Chipera, S. J., & Apps, J. A. (2001). Geochemical Stability of natural zeolites. Reviews in mineralogy and geochemistry, 45.

Cho, M., Maruyama, S., & Liou, J. G. (1987). An experimental investigation of heulandite-laumontite equilibrium at 1000 to 2000 bar P fluid. *Contributions to Mineralogy and Petrology, 97*(1), 43–50.

Coombs, D. S., Ellis, A. J., Fyfe, W. S., & Tayler, A. M. (1959). The zeolite facies, with comments on the interpretation of hydrothermal synthesis. *Geochimica et Cosmochimica Acta, 17*, 53–107.

Deichmann, N., & Baer, M. (2007) Earthquakes in Switzerland and surrounding regions 1996–2006. Report of the Swiss Seismological Service, ETH Zürich.

Eckardt, P. M. (1957). Zur Talgeschichte der Tavetsch und seine Bruchsysteme und jungquartären Verwerfungen. Geologisches Institut Zürich, Dissertation, 120.

Eckardt, P. M., Funk, H., & Labhardt, T. (1983). Postglaziale Krustenbewegungen an der Rhein-Rhone-Linie. *Vermessung, Photogrammetrie, Kulturtechnik, 83*(2), 42–56.

Evans, J. P., Forster, C. B., & Goddard, J. V. (1997). Permeabilty of fault-related rocks, and implications for hydraulic structure of fault zones. *Journal of Structural Geology, 19*(11), 1393–1404.

Fischer, W. (1990). Verschiebungsmessungen im Gebiet Stöckli-Lutersee. Berichte des Instituts für Geodäsie und Photogrammetrie.

Frei, B., & Loew, S. (2001). Störzonen im südlichen Aar-Massiv. *Eclogae Geologicae Helvetiae, 94*(1), 13–28.

Frey, M., Bucher, K., Frank, E., & Mullis, J. (1980). Alpine metamorphism along the geotraverse Basel-Chiasso—A review. *Eclogae Geologicae Helvetiae, 73*, 527–546.

Frey, M., & Mählmann, R. F. (1999). Alpine metamorphism of the Central Alps. *Schweizerische Mineralogische und Petrographische Mitteilungen, 79*, 135–154.

Gapais, D. (1989). Shear structures within deformed granites: Mechanical and thermal indications. *Geology, 17*, 1144–1147.

Glotzbach, C., Reinecker, J., Danišík, M., Rahn, M., Frisch, W., & Spiegel, C. (2010). Thermal history of the central Gotthard and Aar massifs, European Alps: Evidence for steady state, long-term exhumation. *Journal of Geophysical Research, 115*(F3), F03017.

Guerrot, C., & Steiger, R. H. (1991). Variscan granitoids in the Gotthard-massif, Switzerland: Pb-U single zircon and Sr-Nd data. *Terra Abstracts, 3*, 35.

Guilbert, J. M., & Park, C. F., Jr. (1986). *The geology of ore deposits*. New York: WH Freeman and Co.

Hafner, S. (1958). Petrographie des südwestlichen Gotthardmassives (zwischen St. Gotthardpass und Nufenenpass). *Schweizerische Mineralogische und Petrographische Mitteilungen, 38*, 255–362.

Hafner, S., Günthert, A., Burckhardt, C. E., Steiger, R. H., Hansen, J. W. & Niggli, C. R. (1975). Geologischer Atlas der Schweiz 1:25'000, Val Bedretto.

Hardebeck, J. L., & Hauksson, E. (1999). Role of fluids in faulting inferred from stress field signatures. *Science, 285*(5425), 236.

Heer, W. & Jakob, A. (1999). Structural geology and transport modelling for grimsel and aspo. Water-conducting features in radionuclide migration: workshop proceedings, Barcelona, Spain, 10–12 June 1998.

Henley, R. W., & Ellis, A. J. (1983). Geothermal systems, ancient and modern: a geochemical review. *Earth Science Reviews, 19*, 1–50.

Hoagland, J. R., & Elders, W. A. (1978). Hydrothermal mineralogy and isotopic geochemistry of Cerro Prieto geothermal field Mexico. I. Hydrothermal mineral zonation. *Geothermal Resources Council Transactions, 2*, 282–286.

Hobbs, B. E. (1995). Principles involved in mobilization and remobilization. *Ore Geology Reviews, 2*, 37–45.

Jäckli, H. (1951). Verwerfungen jungquartären Alters im südlichen Aarmassiv bei Somvix-Rabius (Graubünden). *Eclogae Geologicae Helvetiae, 44*(2), 332–337.

Jäckli, H. (1957). Gegenwartsgeologie des bündnerischen Rheingebietes. *Beiträger zur Geologischen Karte der Schweiz, geotech. Ser., 36*, 1–136.

James, E. W., & Silver, L. T. (1988). Implications of zeolites and their zonation in the Cajon Pass Deep Drillhole. *Geophysical Research Letters, 15*(9), 973–976.

Jamier, D. (1975). Etude de la fissuration, de l'hydrogéologie et de la géochimie des eaux profondes des massifs de l'Arpille et du Mont-Blanc. PhD, 153.

Jébrak, M. (1992). Les textures intra-filoniennes, marqeurs des conditions hydrauliques et tectoniques. *Chronique de la Recherche Minière, 506*, 55–65.

Jébrak, M. (1997). Hydrothermal breccias in vein-type ore deposits: A review of mechanisms, morphology and size distribution. *Ore Geology Reviews, 12*, 111–137.

Kamber, B. S. (1993). Regional metamorphism and uplift along the southern margin of the Gotthard massif; results from the Nufenenpass area. *Schweizerische Mineralogische und Petrographische Mitteilungen, 73*(2), 241–257.

Kanaori, Y., Kawakami, S.-I., & Yairi, K. (1991). Microstructure of deformed biotite defining foliation in cataclasite zones in granite, central Japan. *Journal of Structural Geology, 13*(7), 777–785.

Kastrup, U., Zoback, M. L., Deichmann, N., Evans, K., Giardini, D. & Michael, A. J. (2004). Stress field variations in the Swiss Alps and the northern Alpine foreland derived from inversion of fault plane solutions. Journal of Geophysical Research 109.

Kipfer, A., & Stuker, P. (1979). Mineralien aus dem Rotondogranit. *Schweizer Strahler, 5*, 45–91.

Klaper, E. M., & Bucher-Nurminen, K. (1987). Alpine metamorphism of pelitic schists in the Nufenen Pass area, Lepontine Alps. *Journal of Metamorphic Geology, 5*(2), 175–195.

Kralik, M., Clauer, N., Holnsteiner, R., Huemer, H., & Kappel, F. (1992). Recurrent fault activity in the Grimsel test site (GTS, Switzerland): revealed by Rb-Sr, K-Ar and tritium isotope techniques. *Journal of the Geological Society, London, 149*, 293–301.

Krasny, J., & Sharp, J. (Eds.). (2007). *Groundwater in fractured rocks (IAH-Selected papers in hydrogeology)*. London: Taylor & Francis.

Kretz, R. (1983). Symbols for rock-forming minerals. *American Mineralogist, 68*(1–2), 277–279.

Labhart, T. P. (1977). *Aarmassiv und Gotthardmassiv*. Schweizerbarth: Stuttgart.

Labhart, T. P. (2005). Erläuterungen zum Geologischen Atlas der Schweiz 1:25000, Val Bedretto, Atlasblatt 68, Bundesamt fuer Umwelt.

Lambert, P., Marquer, D., & Persoz, F. (1992). Structures sur la bordure sud du socle du Gothard; histoire cinématique tertiaire du Val Rondadura (Alpes centrales suisses). *Schweizerische Mineralogische und Petrographische Mitteilungen, 72*(3), 325–334.

Laws, S. (2001). Structural, geomechanical and petrophysical properties of shear zones in the eastern Aar-massif, Switzerland. Geologisches Institut Zürich, PhD, 168.

Laws, S., Eberhardt, E., Loew, S., & Descoeudres, F. (2003). Geomechanical properties of shear zones in the Eastern Aar Massif, Switzerland and their implication on tunnelling. *Rock Mechanics and Rock Engineering, 36*(4), 271–303.

Leu, W. (1985). Geologie der Sedimentzüge zwischen Griessee und Passa del Corno (Nufenengebiet, Wallis) = Géologie des successions de sédiments entre Griessee et Passo del Corno (Région Nufenen, Wallis). *Eclogae Geologicae Helvetiae, 78*(3), 537–544.

Liou, J. G. (1971a). Analcime equilibria. *Lithos, 4*, 389–402.

Liou, J. G. (1971b). P-T stabilities of laumontite, wairakite, lawsonite, and related minerals in the system $CaAl_2Si_2O_8$-SiO_2–H_2O. *Journal of Petrology, 12*, 379–411.

Liou, J. G. (1971c). Stilbite-laumontite equilibrium. *Contributions to Mineralogy and Petrology, 31*, 171–177.

Liou, J. G. (1971d). Synthesis and stability relations for prehnite, $Ca_2Al_2FeSi_3O_{10}(OH)_2$. *American Mineralogist, 56*, 507–531.

Liou, J. G. (1973). Synthesis and stability relations of epidote/$Ca_2Al_2FeSiO_{12}(OH)$. *Journal of Petrology, 14*, 381–413.

Liszkay, M. (1965). Geologie der Sedimentbedeckung des südwestlichen Gotthard-Massivs im Oberwallis. *Eclogae Geologicae Helvetiae, 58*(2), 901–965.

Loew, S., Barla, G. & Diederichs, M. (2010). Engineering geology of Alpine tunnels: Past, present and future. In: A. L. Williams, G. M. Pinches, C. Y. Chin, T. J. MbMorran & C. I. Massey (Eds.), *Geologically active—Proceedings of the 11th IAEG Congress* (pp. 201–253). Auckland: CRC Press.

Loew, S., Lützenkirchen, V., Ofterdinger, U., Zangerl, C., Eberhardt, E. & Evans, K. (2007). Environmental impacts of tunnels in fractured crystalline rocks of the Central Alps. Groundwater in Fractured Rocks, IAH. 9.

Lützenkirchen, V. (2002). Structural geology and hydrogeology of Brittle Fault Zones in the Central and Eastern Gotthard Massif, Switzerland. Geologisches Institut Zürich, PhD, 246.

Maréchal, J.-C. (1998). Les circulations d'eau dans les massifs cristallins alpins et leurs relations avec les ouvrages souterrains. Département de génie civil (GEOLEP), Laboratoire de géologie Lausanne, Ph.D., 296.

Marquer, P. D. (1990). Structures et déformation alpine dans les granites hercyniens du massif du Gotthard (Alpes centrales suisses). *Eclogae Geologicae Helvetiae, 83*(1), 77–97.

Matsuda, T., Omura, K., Ikeda, R., Arai, T., Kobayashi, K., Shimada, K., et al. (2004). Fracture-zone conditions on a recently active fault: Insights from mineralogical and geochemical analyses of the Hirabayashi NIED drill core on the Nojima fault, southwest Japan, which ruptured in the 1995 Kobe earthquake. *Tectonophysics, 378*(3–4), 143–163.

Mercolli, I., Biino, G. G., & Abrecht, J. (1994). The lithostratigraphy of the pre-mesozoic basement of the Gotthard massif: a review. *Schweizerische Mineralogische und Petrographische Mitteilungen, 74*, 29–40.

Merz, C. (1989). L'intrusif Medel-Cristallina (massif du Gothard oriental) Partie I: déformations alpines et relations socle-couverture. *Schweizerische Mineralogische und Petrographische Mitteilungen, 69*, 55–71.

Miller, S. A., Nur, A., & Olgaard, D. L. (1996). Earthquakes as a coupled shear stress-high pore pressure dynamical system. *Geophysical Research Letters, 23*(2), 197–200.

Milnes, A. G. (1974). Structure of the Pennine zone (Central Alps): a new working hypothesis. *Geological Society of America Bulletin, 85*, 1727–1732.

Moore, A. C. (1970). Descriptive terminology for the textures of rock in granulite facies terrain. *Lithos, 3*, 123–127.

Niggli, E. (1970). Alpine Metamorphose und alpine Gebirgsbildung. *Fortschritte der Mineralogie, 47*(1), 16–26.

Nunes, P. D., & Steiger, R. H. (1974). A U-Pb Zircon, and Rb-Sr and U-Th-Pb whole rock study of a polymetamorphic terrane in the Central Alps. *Contributions to Mineralogy and Petrology, 47*, 255–280.

Oberhaensli, R. (1985). Geochemistry of meta-lamprophyres from the Central Swiss Alps. *Schweizerische Mineralogische und Petrographische Mitteilungen, 66*, 315–342.

Oberhänsli, R., Schenker, F., & Mercolli, I. (1988). Indications of Variscan nappe tectonics in the Aar Massif. *Schweizerische Mineralogische und Petrographische Mitteilungen, 68*(3), 509–520.

Ohtani, T., Fujimoto, K., Ito, H., Tanaka, H., Tomida, N., & Higuchi, T. (2000). Fault rocks and past to recent fluid characteristics from the borehole survey of the Nojima fault ruptured in the

1995 Kobe earthquake, southwest Japan. *Journal of Geophysical Research, 105*(B7), 16161–16172.

Parry, W. T., & Bruhn, M. S. (1990). Fluid pressure transient on seismogenic normal fault. *Tectonophysics, 179*, 335–344.

Passchier, C. W., & Trouw, R. A. J. (2005). Microtectonics. Berlin: Springer.

Pennacchioni, G., Di Toro, G., Brack, P., Menegon, L., & Villa, I. M. (2006). Brittle–ductile–brittle deformation during cooling of tonalite (Adamello, Southern Italian Alps). *Tectonophysics, 427*(1–4), 171–197.

Persaud, M., & Pfiffner, O. A. (2004). Active deformation in the eastern Swiss Alps: post-glacial faults, seismicity and surface uplift. *Tectonophysics, 385*(1–4), 59–84.

Pettke, T., & Klaper, E. M. (1992). Zur Petrographie und Deformationsgeschichte des südöstlichen Gotthardmassivs. *Schweizerische Mineralogische und Petrographische Mitteilungen, 72*, 197–211.

Pfiffner, O. A. (2009). *Geologie der Alpen*. Haupt Verlag: Bern Stuttgart Wien.

Priest, S. D. (1993). *Discontinuity analysis for rock engineering*. London: Chapman & Hall.

Robert, F., & Boullier, A. M. (1994). Mesothermal gold-quartz veins and earthquakes. The mechanical involvement of fluids in faulting, pp. 94–228.

Schaltegger, U., & Corfu, F. (1992). The age and source of late Hercynian magmatism in the Central Alps: evidence from precise U-Pb ages and initial Hf isotopes. *Contributions to Mineralogy and Petrology, 111*, 329–344.

Schmid, S. M., Fügenschuh, B., Kissling, E., & Schuster, R. (2004). Tectonic map and overall architecture of the Alpine orogen. *Eclogae Geologicae Helvetiae, 97*(1), 93–117.

Schmid, S. M., Pfiffner, O. A., Froitzheim, N., Schönborn, G., & Kissling, E. (1996). Geophysical-geological transect and tectonic evolution of the Swiss-Italian Alps. *Tectonics, 15*(5), 1036–1064.

Schneider, T. R. (1979). Gotthard Strassentunnel—Geologischer Schlussbericht Nordseite. II.: Geologie., (unpublished report).

Schneider, T. R. (1985) Basistunnel Furka—Geologische Aufnahme des Fensters Bedretto. Brig, Furka-Oberalp-Bahn AG.

Scholz, C. H. (1990). The mechanics of earthquake and faulting. Cambridge: Cambridge University Press.

Seki, Y., Oki, Y., Matsuda, T., Mikami, K., & Okumura, K. (1969). Metamorphism in the Katayama geothermal area, Onikobe, Japan. *Journal of the Geological Society of Japan, 40*, 63–79.

Sergeev, S. A., & Steiger, R. H. (1995). Caledonian and Variscan granitoids of the Gotthard massif: new geochronological and geochemical results. *Schweizerische Mineralogische und Petrographische Mitteilungen, 75*, 315–316.

Sibson, R. H. (1977). Fault rocks and fault mechanisms. *Journal of Geological Society, 133*, 191–213.

Sibson, R. H. (1986). Brecciation processes in fault zones: Inferences from earthquake rupturing. *Pure and Applied Geophysics, 124*, 159–174.

Sibson, R. H. (1992). Implications of fault-valve behaviour for rupture nucleation and recurrence. *Tectonophysics, 211*(1–4), 283–293.

Sibson, R. H. (2000). Fluid involvement in normal faulting. *Journal of Geodynamics, 29*, 469–499.

Snoke, A. W., Tullis, J., & Todd, V. R. (1998) Fault-related rocks: A Photographic Atlas. Princeton: Princeton University Press.

Spear, F. S. (1993). *Metamorphic phase equilibria and pressure-temperature-time paths*. Washington, DC: Mineralogical Society of America.

Stachowiak, G. W., & Batchelor, A. W. (1993). Engineering Tribology.

Steck, A. (1968). Junge Bruchsysteme in den Zentralalpen. *Eclogae Geologicae Helvetiae, 61*(2), 387–393.

Stünitz, H., & Fitz Gerald, J. D. (1993). Deformation of granitoids at low metamorphic grade. II. Granular flow in albite-rich mylonites. *Tectonophysics, 221*, 229–324.

Tanaka, H., Omura, K., Matsuda, T., Ikeda, R., Kobayashi, K., Murakami, M., & Shimada, K. (2007). Architectural evolution of the Nojima fault and identification of the activated slip layer by Kobe earthquake. *Journal of Geophysical Research*, 112/B7.

Thompson, A. B. (1970). Laumontite equilibria and the zeolite facies. *American Journal of Science, 269*, 267–275.

Thompson, A. B. (1971). Analcite-albite equilibria at low temperatures. *American Journal of Science, 271*(1), 79.

Tröger, W. E., Bambauer, H. U., Taborszky, F., & Trochim, H. D. (1982). *Optische Bestimmung der gesteinsbildenden Minerale*. Stuttgart: Schweizerbart.

Tullis, J., & Yund, R. A. (1987). Transition from cataclastic flow to dislocation creep of feldspar: mechanisms and microstructures. *Geology, 15*, 606–609.

Ustaszewski, M., Herwegh, M., McClymont, A. F., Pfiffner, O. A., Pickering, R., & Preusser, F. (2007). Unravelling the evolution of an Alpine to post-glacially active fault in the Swiss Alps. *Journal of Structural Geology, 29*(12), 1943–1959.

Ustaszewski, M., & Pfiffner, O. A. (2008). Neotectonic faulting, uplift and seismicity in the central and western Swiss Alps. Tectonic Aspects of the Alpine-Dinaride-Carpathian System: Carpathian System, 231.

Utada, M. (1965). Zonal distribution of authigenic zeolites in the Tertiary pyroclastic rocks in Mogami district, Yamagata Prefecture. *Tokyo University College General Education Science Paper, 15*, 173–216.

Vincent, M. W., & Ehlig, P. L. (1988). Laumontite mineralization in rocks exposed north of San Andreas fault at Cajon Pass, southern California. *Geophysical Research Letters, 15*(9), 977–980.

Walder, J., & Nur, A. (1984). Porosity reduction and crustal pore pressure development. *Journal of Geophysical Research, 89*(B13), 11539–11548.

Woodcock, N. H., & Mort, K. (2008). Classification of fault breccias and related fault rocks. *Geological Magazine, 145*(3), 435.

Wyder, R. F., & Mullis, J. (1998). Fluid impregnation and development of fault breccias in the Tavetsch basemant rocks (Sedrun, Central Swiss Alps). *Tectonophysics, 294*, 89–107.

Wyss, R. (1985). Die Urseren-Zone zwischen Ulrichen und Oberalppass und ihre Fortsetzung nach Westen und Osten. Geologisches Institut, 169.

Zangerl, C., Loew, S., & Eberhardt, E. (2006). Structure, geometry and formation of brittle discontinuities in anisotropic crystalline rocks of the Central Gotthard Massif, Switzerland. *Eclogae Geologicae Helvetiae, 99*(2), 271–290.

Zeng, Y., & Liou, J. G. (1982). Experimental investigation of yugawaralite-wairakite equilibrium. *American Mineralogist, 67*(9–10), 937–943.